

DISPERSION OF THE BIREFRINGENCE OF CRYSTAL
QUARTZ, MAGNESIUM FLUORIDE, AND SYNTHETIC
SAPPHIRE

by

Michael Gartman Jr.

Copyright © Michael Gartman Jr. 2024

A Dissertation Submitted to the Faculty of the

DEPARTMENT OF OPTICS

In Partial Fulfillment of the Requirements
For the Degree of

MASTER OF SCIENCE
WITH A MAJOR IN OPTICAL SCIENCES

In the Graduate College

THE UNIVERSITY OF ARIZONA

2024

THE UNIVERSITY OF ARIZONA
GRADUATE COLLEGE

As members of the Master's Committee, we certify that we have read the thesis prepared by **Michael Gartman, Jr.**, titled *Dispersion of Birefringence of Crystal Quartz, Magnesium Fluoride, and Sapphire*, and recommend that it be accepted as fulfilling the dissertation requirement for the Master's Degree.



Professor Meredith K. Kupinski

Date: 6/28/2024

Thomas D Milster

Professor Thomas D. Milster


Date: 7/1/2024

David Manzi

David J. Manzi

Date: 7/1/2024

Final approval and acceptance of this thesis is contingent upon the candidate's submission of the final copies of the thesis to the Graduate College.

I hereby certify that I have read this thesis prepared under my direction and recommend that it be accepted as fulfilling the Master's requirement. 



Professor Meredith K. Kupinski
Master's Thesis Committee Chair
Wyant College of Optical Sciences

Date: 7/1/2024

ARIZONA

STATEMENT BY AUTHOR

This dissertation has been submitted in partial fulfillment of requirements for an advanced degree at the University of Arizona and is deposited in the University Library to be made available to borrowers under rules of the Library.

Brief quotations from this dissertation are allowable without special permission, provided that accurate acknowledgment of source is made. Requests for permission for extended quotation from or reproduction of this manuscript in whole or in part may be granted by the head of the major department or the Dean of the Graduate College when in his or her judgment the proposed use of the material is in the interests of scholarship. In all other instances, however, permission must be obtained from the author.

SIGNED: Michael Gartman Jr.

ACKNOWLEDGEMENTS

A full accounting of all the people who helped me get to this point may be impossible, but I certainly plan to try, and any omissions are unintentional on my part.

Thank you everyone for your support and help, whether academically, professionally, personally, or all three.

At the University of Arizona: Dr. Meredith Kupinski, Jeremy Parkinson, Adeline Tai, the other members of the Polarization Laboratory, Jini Kandyil, Dr. Brian Anderson, and Dr. Tom Milster.

At Thorlabs: Bill Donovan, Paul Melone, Dave Manzi, Jim Capelakos, Doug Jenkins, Steve Slinger, Ryan Simmons, Dominic Petrillo, Kelly Dowling, Natasha Mikhailava, Jacleen Carfi, Audrey Biss, Gregoire Lier, Jorge Barria, Will Lowry, Amanda Keeser, Susan Hermes, and last but not least, the entire waveplate team.

Family and friends: Jamie LaCouture, my parents, my siblings, and all other friends and family members.

Everyone listed here helped this work come to fruition, either with a big push or an infinitesimal nudge. Thank you all, I very much appreciate your support, help, advice, encouragement, willingness to share knowledge, provide feedback, try new things, or just put up with me.

DEDICATION

For Jamie

TABLE OF CONTENTS

LIST OF FIGURES	7
LIST OF TABLES	10
ABSTRACT	13
CHAPTER 1 Introduction	14
CHAPTER 2 Background	17
CHAPTER 3 Samples Under Test	20
CHAPTER 4 Experimental Methods	25
4.1 Spectrophotometer Method	25
4.2 Polarimeter Method	29
4.3 Thickness Measurement	31
4.4 Temperature Measurement	33
CHAPTER 5 Experimental Results	36
5.1 Spectrophotometer Results	36
5.2 Polarimeter Results	45
5.3 Tolerances	53
5.4 Temperature Results and Tolerances	60
CHAPTER 6 Conclusions	66
APPENDIX A Additional Tabulated Results	68

LIST OF FIGURES

3.1	Fizeau fringes showing parallelism of a quartz plate prior to measurement in the spectrophotometer. The light bands, rather than the dark, are counted. The three fringes shown here over a 1" aperture corresponds to a parallelism of <3 arcsec. Parallelism is critical for waveplates, as wedge in the plate will result in a variation in retardance across the aperture.	22
3.2	Reflection of N-BK7/index matching fluid/MgF ₂ interface, combined to show reflection of both sides of the plate. Low reflection at the interfaces is necessary to prevent etalon effects [1], which can substantially affect retardance measurements.	23
3.3	Reflection of N-BK7/index matching fluid/sapphire interface, combined to show reflection for both sides of the plate. This graph is similar to Figure 3.2, and shows that the index matching fluid approach can produce similar results in terms of low reflection, even with both different materials and different fluids used.	23
4.1	Transmission peaks and troughs of a quartz waveplate when scanned between two parallel calcite polarizers in a spectrophotometer. Width of peaks can be observed to increase with increase in wavelength. A complete list of all peaks and troughs for this waveplate is available in Table A.4.	26
4.2	Optical system of Perkin Elmer Lambda 950 spectrophotometer used in this work [2]. The dual monochromators used minimize stray light at unintended wavelengths [3].	27
4.3	PAX polarimeter setup. The light enters through a fiber on the top right, is collimated by an aspheric lens, directed onto two turning mirrors, transmitted through a generating polarizer and the sample under test, then detected by the polarimeter on the bottom right. A six-axis mount is used to ensure the sample under test is normal to laser beam.	30
4.4	Bristol Optical Thickness Gauge 157, instrument (left) and collimated output (right).	32
4.5	Absolute physical thickness of samples under test is measured with a Zerodur optical cavity. The 12.7 mm air space and contacted plates are shown here.	33

LIST OF FIGURES – *Continued*

- 5.1 Quartz spectral birefringence difference from the spectrophotometer method. In (a) the difference between fitted equations is on the order of 1.0×10^{-6} over the wavelength range of 320-860 nm. In (b) is shown a comparison of the Sellmeier-type fit and the polynomial fit to the data in the literature [4]. In (c), the orange curve represents the difference between data taken from 210-450 nm and fit to a Sellmeier-type equation and the data in the literature[4], and the blue curve is the difference between the data taken from 210-450 nm and the data taken from 320-860 nm and fit to a Sellmeier-type equation (Eq. 5.1). 38
- 5.2 MgF₂ spectral birefringence difference from the spectrophotometer method. In (a) is the difference between the Sellmeier-type formula (Eq. 5.1) and the polynomial trendline (Eq. 5.2). The fits show a difference of $<3.0 \times 10^{-6}$ from 300-1000 nm. A comparison to the literature [5] for both Sellmeier-type and polynomial equations is shown in (b). Both equations show a difference of $<1.0 \times 10^{-5}$ from 300-1500 nm. Additionally, data were taken in the ultraviolet from 210-450 nm. In (c) these data were compared to both the literature [5] (orange curve), and the data taken from 300-1800 nm (blue curve). 41
- 5.3 Sapphire spectral birefringence difference from spectrophotometer method. Comparison of the fit to the Sellmeier-type equation and the polynomial trendline is shown in (a), the difference between the data in the literature [6] and the two fits is shown in (b). In (c) is shown the difference between the data taken from 210-450 nm and the data taken from 300-1400 nm, and the difference between the data taken from 210-450 nm and the data in the literature [6]. 44
- 5.4 Quartz spectral birefringence difference from the polarimeter method. Difference between data taken using the polarimeter method, and the spectrophotometer method (a) and the literature (b) for quartz. Additionally, the difference between the polarimeter data fit to a Sellmeier-type equation and a polynomial is shown in (c). Even fitting the same data, variation of $<3.0 \times 10^{-6}$ can be seen over the spectrum where data were measured. 47
- 5.5 Fit of MgF₂ birefringence squared to Eq. 5.1. Notable deviations occur at 850 nm, 1549 nm, and 1636 nm. This error may be attributed to anti-reflection coating thickness and source wavelength. 49

LIST OF FIGURES – *Continued*

5.6	MgF ₂ spectral birefringence difference from the polarimeter method. Graph (a) shows the difference between the data taken for MgF ₂ using the polarimeter method (Eq. 5.1, Table 5.10) and the spectrophotometer method (Eq. 5.1, Table 5.1). The difference between the data collected using the polarimeter method and the data in the literature [5] is shown in (b). The difference between fits for data taken with the polarimeter method to an equation of the Sellmeier-type form (Eq. 5.1, Table 5.12), and an equation of the form shown in Eq. 5.4, with the coefficients in Table 5.13 is shown in (c).	50
5.7	Sapphire spectral birefringence difference from the polarimeter method. Difference in birefringence of sapphire between data obtained from the polarimetric method (Eq. 5.3, Table 5.14) and the spectrophotometer method (Eq. 5.3, Table 5.7) is shown in (a). Difference between the polarimeter method and the data in the literature [6] is shown in (b). Difference between birefringence for sapphire using Sellmeier-type (Eq. 5.3, Table 5.14) and polynomial fits (Eq. 5.2, Table 5.15) is shown in (c).	52
5.8	The three largest sources of uncertainty in the spectrophotometer method. In (a) is the variation of birefringence error due to dual effects of non-collimated beam versus wavelength characterized in Table 5.16. In (b) is the effect of wavelength tolerance in the instrument. Discontinuity is due to grating and detector change. Curves are shown for one sign only, but are \pm , so should be understood as rotated about the abscissa. Potential error due to physical thickness tolerance is shown in (c). Graphs are color coded: blue (quartz), orange (MgF ₂), gray (sapphire).	57
5.9	Potential total birefringence error for all three materials due to uncertainty in spectrophotometer. Discontinuity is where the error changes, due to grating and detector change in the instrument. The blue curve is the upper bound of the tolerance for all three materials, and the orange curve is the lower bound.	58
5.10	Potential sources of error for polarimeter method. Discontinuities in graphs (a) and (f) are due to change in polarimeter used. Variation in error with wavelength in graph (b) due to different thicknesses of parts being used. Graphs are color coded: MgF ₂ (orange), quartz (blue), and sapphire (gray).	61
5.11	Change in retardance with temperature for: (a) quartz, (b) MgF ₂ , and (c) sapphire. Sapphire has a positive slope because the birefringence is negative.	63

LIST OF TABLES

4.1	Thicknesses of parts tested for retardance in spectrophotometer, as well as start and ending wavelengths used.	25
4.2	Thicknesses of parts tested for retardance in spectrophotometer over ultraviolet range, as well as start and ending wavelengths used.	29
4.3	Thicknesses of parts tested for γ and $d\beta/dT$	35
5.1	Quartz dispersion coefficients based on spectrophotometer data, fit to a Sellmeier-type equation, as shown in Eq. 5.1.	36
5.2	Coefficients of quartz based on spectrophotometer data fit to Eq. 5.2.	37
5.3	Quartz dispersion coefficients based on spectrophotometer data in the ultraviolet and lower visible range; fit to Eq. 5.1.	39
5.4	MgF ₂ dispersion coefficients based on spectrophotometer data, fit to Eq. 5.1.	40
5.5	MgF ₂ dispersion coefficients based on spectrophotometer data fit to Eq. 5.2.	42
5.6	MgF ₂ dispersion coefficients based on spectrophotometer data in the ultraviolet and lower visible range fit to Eq. 5.1.	42
5.7	Sapphire dispersion coefficients based on spectrophotometer data, fit to Eq. 5.3.	42
5.8	Sapphire dispersion coefficients based on spectrophotometer fit to Eq. 5.2.	43
5.9	Sapphire dispersion coefficients in UV based on spectrophotometer fit to Eq. 5.3.	43
5.10	Quartz dispersion coefficients based on polarimeter data fit to Eq. 5.1.	46
5.11	Quartz dispersion coefficients based on laser and polarimeter fit to Eq. 5.2.	48
5.12	MgF ₂ dispersion coefficients based on polarimeter data fit to Eq. 5.1.	48
5.13	MgF ₂ dispersion coefficients based on laser data fit to Eq. 5.4.	49
5.14	Sapphire dispersion coefficients (Eq. 5.3) based on polarimeter data.	51
5.15	Sapphire dispersion coefficients based on polarimeter data fit to Eq. 5.2.	53
5.16	Total change in effective thickness of plates in spectrophotometer due to effects in Tables A.12 and A.13.	55
5.17	Birefringence error due to potential temperature error in sensor.	56

LIST OF TABLES – *Continued*

5.18	Comparison of $d\beta/dT$ and γ for quartz in the literature and this work. Toyoda reports a value of $d\beta/dT$, whereas the value of $d\beta/dT$ for Etzel is calculated from parameters provided in that paper. Etzel does provides a value of γ from the data reported in Toyoda, and that value is reproduced here.	64
5.19	MgF ₂ temperature dependence where γ cannot be computed for Duncanson, as $d\beta/dT$ for that work is calculated by the deviation from a prism, rather than a retardance measurement.	65
5.20	Comparison of $d\beta/dT$ and γ for sapphire. $d\beta/dT$ for Kraemer not reported, and cannot be calculated, as there is no quoted data in that work [7]. γ cannot be computed for Yang and DeFranzo, as $d\beta/dT$ for that work is calculated by the deviation from a prism, rather than a retardance measurement. Sapphire has $d\beta/dT$ and γ with opposing signs, as the retardance of sapphire is negative.	65
A.1	Change in retardance for quartz part with temperature, showing measured temperature in °C and measured retardance in waves.	68
A.2	Change in retardance for magnesium fluoride part with temperature. Note significantly lower change in magnitude compared to quartz (Table A.1) and sapphire (Table A.3).	68
A.3	Change in retardance for sapphire part with temperature. Values of retardance are negative as sapphire is a negative crystal. Note similarity in terms of magnitude of change in the retardance to quartz (Table A.1).	68
A.4	Extrema of quartz measurement in spectrophotometer, with number of waves at that wavelength per the literature [4], and number of waves as determined in this work. Difference in significant figures is due to definition of extrema – a peak is exactly a full wave, and a trough is exactly a half wave.	69
A.5	Spectral birefringence of quartz from polarimetric measurements.	70
A.6	Comparison of measured birefringence with calculated birefringence from Sellmeier fit using Eq. 5.1 and Table 5.10.	70
A.7	Spectral birefringence of MgF ₂ from polarimetric measurements.	71
A.8	MgF ₂ comparison between Sellmeier fit (Eq. 5.1, Table 5.12) and measured birefringence data. These data show a fit $<3.0 \times 10^{-6}$ prior to 850 nm, and a fit on the order of 2.0×10^{-5} at the last two data points, of 1549 nm and 1636 nm.	71
A.9	Laser wavelengths and birefringence measurements for sapphire measured using polarimeter method.	72

LIST OF TABLES – *Continued*

A.10 Comparison of measured birefringence values and Sellmeier fit (Eq. 5.3, Table 5.14) for sapphire data taken on polarimeter. Fit is $<1.0 \times 10^{-6}$ for all wavelengths measured.	72
A.11 Wavelengths tested on AxoScan and PAX polarimeters	73
A.12 Change in effective thickness in microns of plates used in spectrophotometer due to non-collimated beam, at both 320 and 860 nm.	73
A.13 Change in effective thickness in microns of plates used in spectrophotometer due to decrease in birefringence.	73
A.14 R^2 value of retardance versus temperature trendlines for materials. Lower value of R^2 for MgF_2 may be due to lower thickness of part used compared to other materials (see Table 4.3).	73

ABSTRACT

Accurate methods for characterizing birefringence are crucial for the design and production of optics that manipulate polarized light, especially for waveplates that require precise thickness to achieve a specific retardance at a given wavelength. Typically, the tolerances for polishing waveplates are approximately $\pm 0.25 \mu m$. This thesis characterizes the birefringence of three commonly used waveplate materials: crystal quartz, magnesium fluoride, and synthetic sapphire and compares values of two independent experimental methods. Dispersion formulae for each material are established and verified against existing literature. The results indicate a high level of agreement between the two experimental methods, showing consistency within 1.0×10^{-5} for birefringence values across the wavelength range of 300-1800 nm. Furthermore, the experimental data align closely with the published values, with deviations within 1.0×10^{-5} for quartz and magnesium fluoride and within 3.0×10^{-5} for sapphire.

CHAPTER 1

Introduction

Accurate knowledge of the birefringence of crystalline materials is critical for designing waveplates and other polarization sensitive optics. Crystal quartz, magnesium fluoride, and synthetic sapphire all feature a broad transparency range from the UV through the mid-infrared and are commonly used birefringent materials for applications in these regions. While the birefringence of each of these materials has been previously reported in the literature [4, 5, 6], using the minimum deviation method of measuring refractive index, this work explores two methods of measuring the dependence of birefringence on wavelength directly.

Method one uses a commercial off-the-shelf spectrophotometer with additional polarizing elements. Method two uses commercial polarimeters illuminated with various laser sources. These two independent methods are then compared both with each other, as well as with the existing literature.

Accurate values of birefringence for all three materials in this work are necessary for polishing waveplates. Paradoxically, although birefringence is the difference of two refractive indices, it needs to be an order of magnitude or more accurate than refractive index data – the tightest tolerance optical glass manufacturers quote on refractive index is 1×10^{-4} [8]. However, a multi-order quarter waveplate at 632.8 nm of roughly 0.78 mm thickness with a birefringence error on the order of 1×10^{-4} would produce an ellipticity of 0.63, whereas an error on the order of 1×10^{-5} would lead to an ellipticity of 0.96, and 5×10^{-6} would produce an ellipticity of 0.98. Therefore, an error in the value of birefringence would need to be $<1 \times 10^{-5}$ for most waveplate applications.

The first experimental method is the simplest – it involves placing the sample under test between parallel polarizers in a spectrophotometer and then measuring the transmission function of the sample over the wavelength range of interest. This

method has been documented previously in the literature [9]. Since the spectrophotometer uses a white light source (both a deuterium and a halogen lamp) as well as dual grating-based monochromators, this method is closer to sampling a continuous spectrum rather than measuring at discrete light sources. However, it is limited by the use of a non-collimated beam (which can produce angle-of-incidence artifacts), the potential for stray light in the monochromator assembly, limitations of the mechanical slits for discriminating against adjacent wavelengths, and finally alignment issues. The spectrophotometer used in this work has a wavelength range of 175-3300 nm, and a wavelength resolution of ± 0.08 nm.

The second method involves measuring the retardance of samples of each material using a commercial polarimeter at various discrete wavelengths with laser sources. This is one of the recommended applications for one of the polarimeters used [10]. An optical spectrum analyzer was used to measure the wavelength of the source. This method has the advantages of using a collimated beam, accurately determining the wavelength used for the retardation measurement, and, depending on the polarimeter used, fully characterizing the optical characteristics of the material. Disadvantages include the need for samples with anti-reflection coatings, as it is documented in the literature that etalon effects can significantly affect retardance measurements [1]. Uncoated samples studied in this work will have Fresnel reflections large enough to produce those effects, so samples with anti-reflection coatings were used to avoid this issue.

While parts were tested under similar environmental conditions, temperature measurements were taken at the beginning and end of each measurement and were recorded in order to allow normalization of birefringence to 20° C. This adjustment was performed to better fit the data to a model as both refractive index and birefringence are temperature dependent. For the materials studied in this work, dn/dT is not equal for the ordinary and extraordinary rays [11, 12, 13], which necessitates a knowledge of how birefringence changes with temperature. Data were adjusted to 20° C to allow ease of comparison across materials, as well as to facilitate comparisons to the literature.

Finally, the two different methods herein were compared to each other, as well as to previously published data. It was found that for quartz, the two methods were consistent with each other within $<3 \times 10^{-6}$ over the wavelength range where measurements for both methods were taken, within $<1 \times 10^{-5}$ for magnesium fluoride, and within $<4 \times 10^{-6}$ for sapphire.

Chapter 2 of this work covers necessary background material, as well as a brief overview of birefringence. Chapter 3 describes the samples under test. The experimental methods, including those used to measure thickness of the samples tested, as well as the techniques used to quantify change in retardance with temperature are described in Chapter 4. Chapter 5 reports the experimental results.

CHAPTER 2

Background

Accurate knowledge of the birefringence of anisotropic materials is critical to the design of optics intended to manipulate polarized light. This information is particularly important for waveplates (also known as retarders or phase shifters) since they directly rely on the birefringence of the material used, unlike crystal polarizers, which depend on the ordinary and extraordinary refractive indices separately, such as in a Glan-type polarizer design.

Commonly used materials for waveplates include crystal quartz (also known as α -quartz), magnesium fluoride, and sapphire. There are a number of examples of measurement of both ordinary and extraordinary refractive indices in the literature for commonly-used birefringent materials [4, 5, 6], but the calculated birefringence from these references have large error bars, typically reported on the order of 1.0×10^{-5} , either from the error bars on the measurement itself, or the curve fit to the data.

The data in the previous studies were collected using the minimum deviation method – a light source (often a gas-discharge lamp which emits at one or a limited number of wavelengths) is collimated and directed at a prism of the material in question. That prism is then rotated, and the angle of minimum deviation is recorded, from which the index of refraction can be calculated. This technique is a common method used to test refractive index [14] and can be extended to birefringent materials; in that instance, a generating polarizer is included in the optical path prior to the light being incident on the prism, and with the optic axis of the material perpendicular to the triangular faces of the prism, while dividing the angle of refraction.

In this work, we evaluate the birefringence of the listed materials using two independent methods, which do not depend on the minimum deviation method

described above, and compare the results of these methods with each other as well as with existing literature. By using methods that directly measure the birefringence, we aim to achieve a model fit better than previously achieved in the literature.

Optically isotropic materials have one refractive index. The refractive index is the speed of light in a vacuum divided by the speed of light in that particular medium. Light travels at the same group velocity in an isotropic material regardless of orientation of the material, direction of light propagation, or polarization state. In contrast, anisotropic materials have more than one refractive index, meaning the velocity of light in such a material is dependent on the direction of propagation of the input light. This effect will cause light propagating in such a material to split into two modes, which will propagate at different speeds and therefore refract at different angles [15].

Birefringence was first identified by Bartholinus in 1669, in optical calcite. For materials with two refractive indices (uniaxial crystals), the refractive indices are by convention called the ordinary (n_o) and the extraordinary indices (n_e). The difference between the two is the birefringence, commonly represented by $\beta = n_e - n_o$. When β is positive ($n_o < n_e$), the material is referred to as a positive crystal. When it is negative ($n_o > n_e$), the material is referred to as a negative crystal. Quartz and magnesium fluoride are positive crystals, and sapphire is a negative crystal.

Birefringence is not constant with wavelength – n_o and n_e disperse at different rates for the materials studied in this work, causing the value of birefringence to vary significantly even across relatively small (tens of nanometers) changes in wavelength. To that end, the birefringence is evaluated in this work across a spectrum stretching from roughly 300 nm to 1800 nm, depending on material.

Of the previous works we compared data taken in this work to, Dodge [5] and Malitson [6] provide values of birefringence indirectly – they report n_o and n_e for the materials studied, and the birefringence from the difference between the two (or the difference between the curves fitted to the refractive indices). Ghosh [4], however, reports both a dispersion formula for each n_o and n_e , but also a dispersion formula for β . It is to the latter that we compare to our data in this work, as it more closely

fits the data reported in the literature than the difference between the dispersion formulae of the indices.

Birefringence varies with temperature – much like with dispersion, for the materials in this work, $dn_o/dT \neq dn_e/dT$, so the temperature the material is subjected to must be considered as well. In this work, the change in the birefringence with temperature for all three materials is studied over the temperature range of around room temperature to approximately 45° C at 632.8 nm.

Birefringence is due to the physical structure of the material in question – the materials discussed in this work (and all birefringent materials) do not have a cubic crystal structure; quartz and sapphire are trigonal [16, 17], and MgF_2 is tetragonal [18].

The optic axis of an anisotropic material is the direction parallel to which any propagating ray only experiences the ordinary refractive index. In all other directions of the material, any propagating light experiences both refractive indices. While this fact can be exploited to make polarizers, this work is concerned with waveplates, which are typically produced by cutting and polishing optical materials to maximize birefringence – that is, by producing plane parallel plates with the optic axis in the plane of the plate.

With the optic axis of a birefringent material in the plane of the plate, the difference in optical path length between the two separate modes is maximized [15]. This is commonly known as an A-plate configuration, as opposed to a C-plate configuration, which is designed to minimize birefringence. This difference in optical path length produces the retardance associated with birefringent materials.

CHAPTER 3

Samples Under Test

Crystal quartz, magnesium fluoride, and sapphire are among the most commonly used crystals to manufacture waveplates. All three materials are birefringent, which is a necessary condition to produce waveplates, and are readily available. Additionally, the birefringence values of these materials are neither too high (such as calcite, where one full wave of retardance at 632.8 nm is $3.7 \mu\text{m}$) nor too low (such as apophyllite, where a $\lambda/4$ waveplate at 600 nm would be 15 mm thick [19]).

However, while the materials under study are each less birefringent than others, they are still more birefringent than may be desirable, as true zero-order waveplates (that is, single plates providing exactly 0.25 or 0.5 waves of retardance) of these materials are relatively thin and are not commonly produced outside of the mid-infrared (MIR) region. More commonly used are multi-order waveplates, zero-order waveplates, or achromatic waveplates made from a combination of two materials.

Crystal quartz is the most commonly used of the three materials, as it has a broad transparency range, with minimal absorption from the UV ($< 190 \text{ nm}$) to the MIR ($> 2.8 \mu\text{m}$) [20], and is reasonably hard (7 on the Mohs scale) which makes it relatively easy to polish to a high-quality finish. While quartz does occur naturally, significant demand from the electronics industry means that material of high optical quality is readily available and inexpensive, obviating any need for natural material (which can have defects rendering it unsuitable for precision applications [21]). For these reasons, quartz is typically the preferred material for manufacturing waveplates in the UV, visible, near-infrared (NIR), and lower MIR regions. A disadvantage of quartz is that it is optically active, even in directions perpendicular to the optic axis of the crystal. This effect results in a slight rotation of the polarization of incoming polarized light, even when its orientation is parallel to the optic axis [22].

Magnesium fluoride is softer than quartz (6 on the Mohs scale) and more difficult

to polish to a high optical quality (often showing streaks even after careful polishing), but has a broader transparency range than quartz (< 120 nm in the UV and $> 8 \mu\text{m}$ in the MIR [18]). It is often paired with quartz to produce achromatic waveplates in the visible, NIR, and NIR/telecom regions. It is also used for multi-order and zero-order waveplates deeper in the UV or farther into the MIR than quartz due to its greater range of transparency.

Sapphire is less commonly used to make waveplates than either crystal quartz or magnesium fluoride, but has some advantages when compared with both, with its high hardness (9 on the Mohs scale), and resistance to both chemicals and higher temperatures. Sapphire is thermally stable from cryogenic temperatures until its melting point which is $>2000^\circ\text{C}$ [23]. However, due to its high hardness, sapphire is more difficult to process than either crystal quartz or magnesium fluoride, requiring specialized techniques. Its transmission spectrum is broader than quartz, but not as broad as that of magnesium fluoride, ranging from <190 nm in the UV to $>5 \mu\text{m}$ in the MIR [23]. It has been used to make multi-order and zero-order waveplates (often in the MIR) in applications where durability is a desired characteristic, as well as achromatic waveplates in the UV, visible, and NIR regions when paired with quartz.

Initial samples of all three materials for testing using the spectrophotometer method were taken from waveplate production lots, and were parts that had been scrapped for cosmetic reasons (e.g. edge chips, scratches, digs) that will not affect the birefringence measurement. Parts had not been coated, were parallel to <3 arcsec, as verified with a Fizeau interferometer (an example image can be seen in Figure 3.1, showing three fringes on a 1" diameter quartz plate), and had a transmitted wavefront error of $<\lambda/10$ rms, as measured on a phase shifting interferometer. Nominal orientation of the optic axis to the surface of the plates were <6 arcmin for quartz and magnesium fluoride, and <12 arcmin for sapphire, per the raw material suppliers.

Quartz samples in the polarimetric measurements (for both polarimeters) were taken from standard waveplate production lots. Unlike the samples used in the

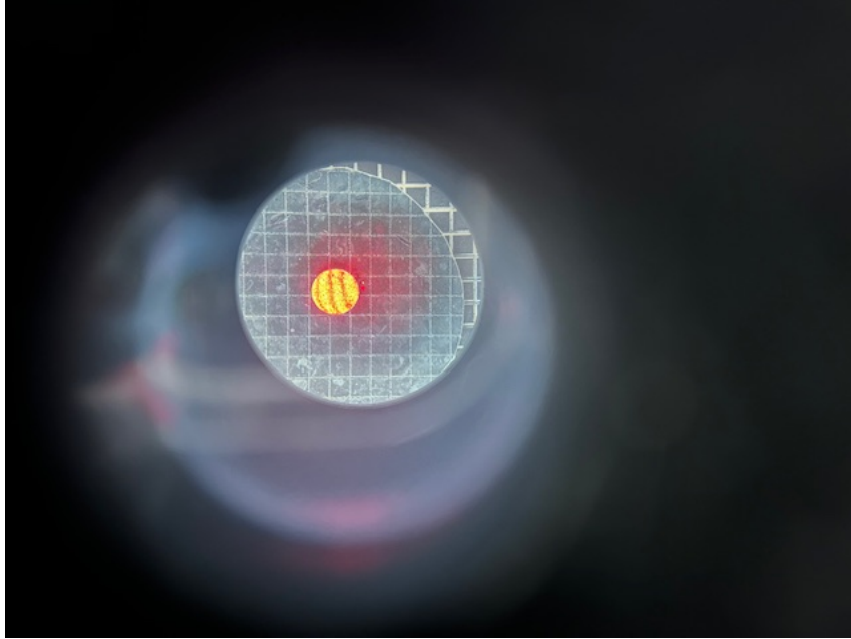


Figure 3.1: Fizeau fringes showing parallelism of a quartz plate prior to measurement in the spectrophotometer. The light bands, rather than the dark, are counted. The three fringes shown here over a 1" aperture corresponds to a parallelism of <3 arcsec. Parallelism is critical for waveplates, as wedge in the plate will result in a variation in retardance across the aperture.

spectrophotometer, these were production parts that were anti-reflection coated at or around the test wavelength. Using coated parts reduced the likelihood of any artifacts in the retardance measurement induced by etalon effects [1]. Their parallelism, transmitted wavefront error, and orientation of the optic axis were similar to the rejected parts detailed previously.

Magnesium fluoride samples for the polarimetric measurements were uncoated for measurements <800 nm, and used parts that had been coated with appropriate broadband anti-reflection coatings for measurements >800 nm. The uncoated parts were sandwiched between N-BK7 windows that had a broadband anti-reflection coating on one side and index matching fluid at the interface between the uncoated side of the window and the MgF_2 part. Although N-BK7 and MgF_2 have different refractive indices (n_d of N-BK7 is 1.517, and n_d for MgF_2 is 1.378 for the ordinary ray), the index of the index matching fluid was nearly identical to that of N-BK7,

so the overall transmission of the assembled system was approximately 98% over the range of 400-800nm. Figure 3.2 shows the combined theoretical reflection of the N-BK7/index matching fluid/MgF₂ interface for both sides of the MgF₂ part, meaning the loss due to Fresnel reflections at the fluid interface were <0.5% over the wavelength range where the above configuration was used.

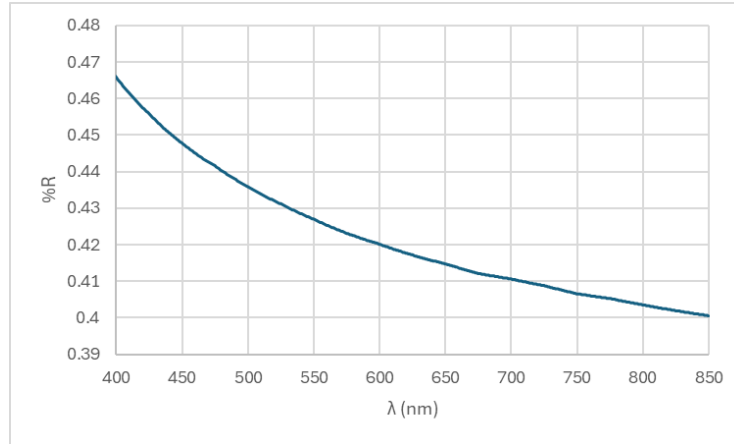


Figure 3.2: Reflection of N-BK7/index matching fluid/MgF₂ interface, combined to show reflection of both sides of the plate. Low reflection at the interfaces is necessary to prevent etalon effects [1], which can substantially affect retardance measurements.

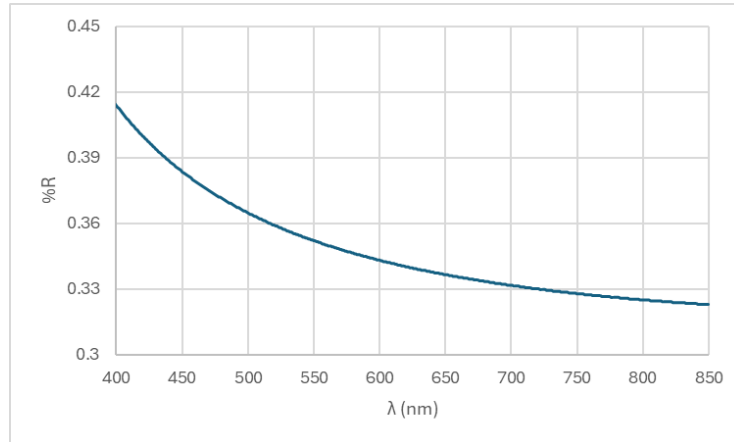


Figure 3.3: Reflection of N-BK7/index matching fluid/sapphire interface, combined to show reflection for both sides of the plate. This graph is similar to Figure 3.2, and shows that the index matching fluid approach can produce similar results in terms of low reflection, even with both different materials and different fluids used.

Sapphire samples in the polarimetric measurements were uncoated, and, like the MgF_2 samples, were sandwiched between N-BK7 windows that had a broadband anti-reflection coating on one side, and index matching fluid between the uncoated surface of each window and the sapphire, in order to prevent etalon effects. Given that N-BK7 and sapphire have markedly different indices (n_d of N-BK7 is 1.517, and n_d for sapphire is 1.768 for the ordinary ray), an index matching fluid with an intermediate index was selected ($n_d = 1.61$). This construction resulted in reflection losses of approximately 0.4% for the N-BK7-fluid-sapphire interface total, allowing high transmission. A curve showing expected reflection losses for both interfaces is shown in Figure 3.3. As can be seen, reflection losses for both interfaces combined are $<0.45\%$ for the entire wavelength range measured.

CHAPTER 4

Experimental Methods

4.1 Spectrophotometer Method

The birefringence of the materials of interest was measured and compared through two unrelated and independent experimental methods. The first method involved placing polished samples of a known thickness of each material in a commercial spectrophotometer (PerkinElmer Lambda 950, the optical system of which is shown in Figure 4.2) between two calcite polarizers placed in the sample compartment. The calcite polarizers had their transmission axes parallel, and the plate under test is cut as an A-plate. The part is rotated about the beam path so that the optic axis of the part is oriented at roughly 45° to the axes of the polarizers. As the retardance of the part varies with wavelength, stepping through wavelengths produces a squared sinusoidal curve (c.f. Malus' Law – a waveplate between two crossed polarizers will produce similar results to two polarizers where the analyzer is rotated), which can be seen in Figure 4.1. The temperature was recorded at both the beginning and the end of each scan, as birefringence has a dependence on temperature for the materials under study. The thickness of the part used, as well as the starting and ending wavelength for each material is shown in Table 4.1.

For such a curve, the individual peaks are transmission maxima, and represent

Material	Quartz	MgF ₂	Sapphire
Physical thickness	1.0122 mm	1.8707 mm	3.1964 mm
Start wavelength	320 nm	300 nm	300 nm
End wavelength	860 nm	1800 nm	1400 nm

Table 4.1: Thicknesses of parts tested for retardance in spectrophotometer, as well as start and ending wavelengths used.

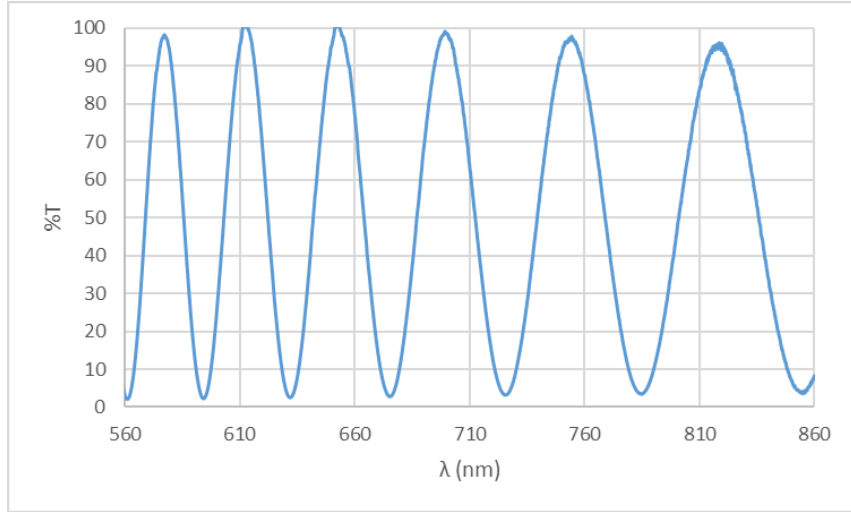


Figure 4.1: Transmission peaks and troughs of a quartz waveplate when scanned between two parallel calcite polarizers in a spectrophotometer. Width of peaks can be observed to increase with increase in wavelength. A complete list of all peaks and troughs for this waveplate is available in Table A.4.

full (i.e. integer) numbers of waves of retardance. The troughs are transmission minima, and represent half-integer numbers of waves. For crossed polarizers, the situation would be reversed – peaks would be half-integer values, and troughs would be half-integer values. Transmission maxima and minima are not exactly 100% and 0%, respectively, due to the optic axis of the sample under test not being exactly at 45° to the axes of the polarizers, or because of slight alignment error in the axes of the polarizers. These alignment issues are not critical, as imperfect alignment affects the height of the transmission maxima and minima, not their positioning [24].

Wavelength was scanned from high to low, in 0.1 nm steps with a 0.2 nm slit width (a slit width of twice the step size is recommended by Perkin Elmer when wavelength resolution is desirable, as it is here). Parts were aligned using the instrument’s white light alignment beam, and back reflecting the beam upon itself. (This alignment was accomplished by obscuring a portion of the top of the beam with paper, in order to observe both the beam entering the sample compartment, as well as the back reflection from the sample.) The alignment beam was turned off

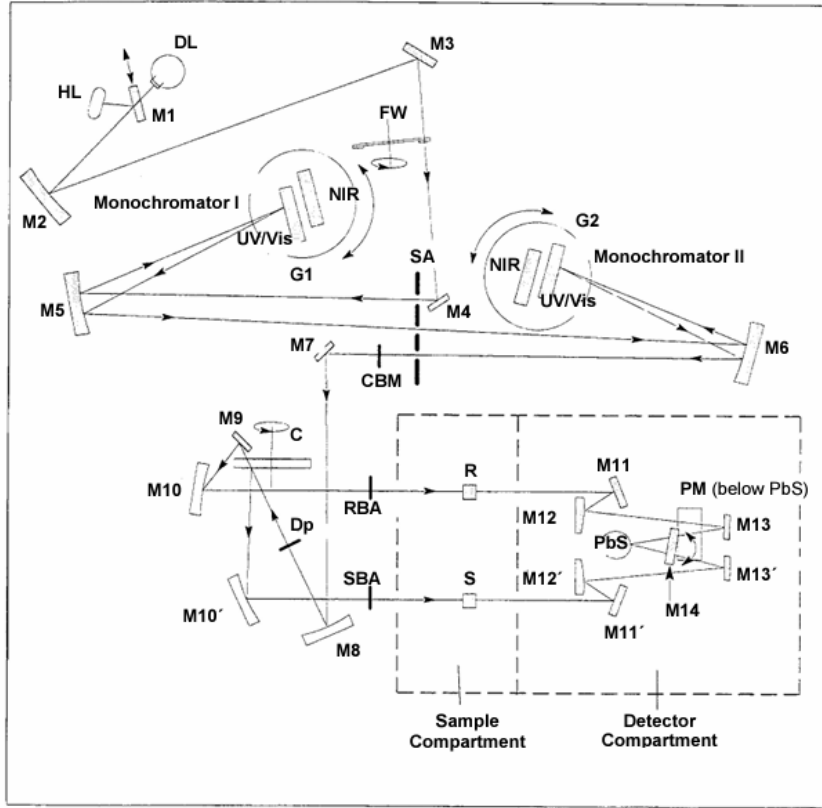


Figure 4.2: Optical system of Perkin Elmer Lambda 950 spectrophotometer used in this work [2]. The dual monochromators used minimize stray light at unintended wavelengths [3].

prior to starting the measurement.

The optical system of the spectrophotometer used is shown in Figure 4.2 for reference. Parts were placed in the sample compartment, in the sample beam.

Once the curve had been produced, the locations of the transmission maxima and minima were located using a Python program which used the `find_peaks_cwt` function in the SciPy package, after which the location of the maxima and minima were double checked manually. The birefringence can be calculated once the number of waves at each extrema is determined if the physical thickness of the part is known,

$$\beta = \frac{\lambda \times \text{Waves}}{t}, \quad (4.1)$$

where β is the birefringence, t is the physical thickness of the part in question, and λ is the wavelength. As the number of waves at any extremum cannot be computed from the transmission curve, the number of waves at one extremum was calculated using previous literature [4, 5, 6] and that was used to determine the integer values of the other extrema for that material. (As each extremum is by definition 0.5 waves from the extrema on either side of it.)

After the extrema are assigned integer or half-integer values, birefringence at each extremum was calculated. The temperature during each scan was averaged, and the birefringence was adjusted to 20° C (68° F), to allow one-to-one comparison across datasets. The values and methods of obtaining $d\beta/dT$ for the materials under study here are discussed in a later section, and are also available in the literature [12, 25]. The adjusted birefringence was plotted against inverse wavelength. When the plot of birefringence versus inverse wavelength was obtained, a curve was fit to the data, the equation of which would allow birefringence for any arbitrary wavelength, rather than merely one of the extrema, to be calculated. Curves were fitted using the polynomial trendline function in Microsoft Excel. For fitting to Sellmeier-type equations, the birefringence was squared and plotted against wavelength and fit in Python with a program that used the `curve_fit` function in SciPy.

Data were also taken using the spectrophotometer method deeper in the ultraviolet region. The physical thickness of the parts used is shown in Table 4.2. While the scans were all taken over the wavelength range of 210-450 nm (210 nm is the nominal lower limit of the polarizer used as a generator), absorption in the polarizers used prevented fitting of curves below 215 nm. Due to the increase in dispersion in the ultraviolet region displayed by all three materials in this study, the steps were the minimum allowed by the instrument – 0.03 nm. The slit width was twice the value of the step size, which allows for fine wavelength resolution per the manufacturer, as mentioned previously. Additionally, thinner parts were selected to allow finer resolution of wavelength-related features.

Material	Quartz	MgF2	Sapphire
Physical thickness	0.7519 mm	0.6322 mm	0.8113 mm
Start wavelength	210 nm	210 nm	210 nm
End wavelength	450 nm	450 nm	450 nm

Table 4.2: Thicknesses of parts tested for retardance in spectrophotometer over ultraviolet range, as well as start and ending wavelengths used.

4.2 Polarimeter Method

The second method of measuring birefringence involved measuring retardance of plane parallel plates of each material, of known thicknesses with the optic axis in the plane of the plate (A-plate configuration) on a commercial polarimeter. Two polarimeters were used – an Axometrics AxoScan, which is a Mueller matrix polarimeter, and has a wavelength range of 400-1000 nm, and a Thorlabs PAX1000IR2, which is a Stokes polarimeter, and has a wavelength range of 900-1700 nm. An image of the PAX polarimeter setup is shown in Figure 4.3. In addition, the wavelength of the laser used was determined during the test by directing a portion of the laser output to an optical spectrum analyzer (Thorlabs OSA201C for wavelengths between 400-1000nm, Thorlabs OSA202 for wavelengths between 1000-1650nm.) These instruments both use a Michelson interferometer and Fourier transform to obtain the spectrum of the input source.

For the second method, both polished plates as well as plates that had been both polished and coated with an anti-reflection coating at the appropriate wavelength were used. Plates that were not anti-reflection coated were placed between two windows that had a broadband anti-reflection coating on one side, and were placed in contact with the uncoated side of the windows using index matching fluid, as detailed previously. Different index matching fluids were used, depending on the material under test. The use of anti-reflection coatings helps to suppress etalon effects that can otherwise significantly affect retardance measurements [1].

Retardance measurements for each plate were taken continuously over long periods of time to allow the plate being measured to come to thermal equilibrium

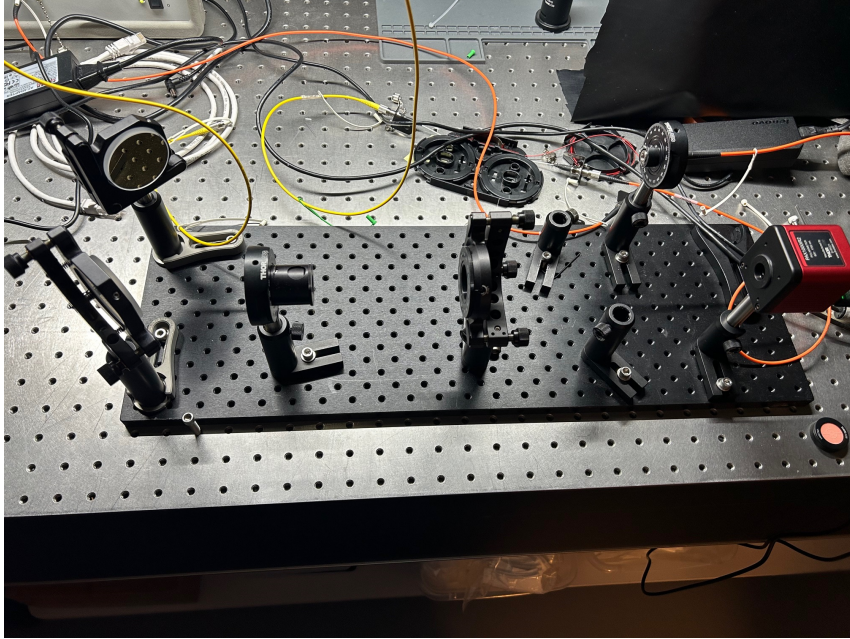


Figure 4.3: PAX polarimeter setup. The light enters through a fiber on the top right, is collimated by an aspheric lens, directed onto two turning mirrors, transmitted through a generating polarizer and the sample under test, then detected by the polarimeter on the bottom right. A six-axis mount is used to ensure the sample under test is normal to laser beam.

with the environment. It was determined when the parts had come to thermal equilibrium by monitoring the retardance measurement in real time and recording the measurement when minimal change ($<0.1^\circ$ of retardance, or $\lambda/3600$ in waves) was noted over the span of approximately two minutes. These measurements (with approximately one measurement taken every second) were then averaged. The temperature of the ambient environment was recorded at the beginning and the end of each measurement.

This measurement procedure was repeated for two additional plates at each wavelength for each material. The wavelengths of the lasers used to test the parts on the polarimeters are available in Table A.11. Wavelength values were obtained by a convolution of the output spectrum of the wavelength with the intensity, as some laser sources displayed non-single mode operation.

Birefringence and wavelength measurements for each laser source were averaged

to produce one value for wavelength and one value for birefringence for that wavelength. Following the averaging, the values of birefringence were temperature adjusted to 20° C, and a curve to allow calculation at arbitrary wavelengths was fit to the birefringence versus wavelength values for each material, using both a polynomial fit (Eq. 5.2), and a Sellmeier equation (Eq. 5.1).

After data were taken for each method, birefringence values were compared across methods by computing the difference between the dispersion formulas generated at various wavelengths.

4.3 Thickness Measurement

In order to measure birefringence, an accurate determination of physical thickness must first be made, given that retardance is dependent on the physical thickness of the part in question, as shown in Eq. 4.1.

A contact-based physical measurement of the thickness of the plate is not sufficient – typical drop gauge accuracy of $\pm 1 \mu m$ [26] would result in a retardance accuracy of $\lambda/35$ at 632.8 nm for a multi-order waveplate, whereas typical retardance accuracy for multi-order waveplates is $\lambda/100$ or greater at the design wavelength.

Therefore, physical thickness of the plates in this work were measured with a commercial optical thickness gauge (Bristol 157), which is a non-contact method that relies on optical path length. This instrument is accurate to $\pm 0.1 \mu m$ [27], which would result in a retardance accuracy of $\lambda/350$ at 632.8 nm, which is within the range of accuracy necessary to not have thickness error entirely driving any uncertainty in retardance or birefringence.

The non-contact measurement measures the optical thickness of a sample under test, which requires an accurate group index measurement, as the instrument uses a broadband superluminescent diode. Since the parts under test are birefringent, an accurate thickness measurement can only be obtained by isolating each refractive index – that is, with polarized light.

Polarizers were positioned below the light source on the optical thickness gauge,

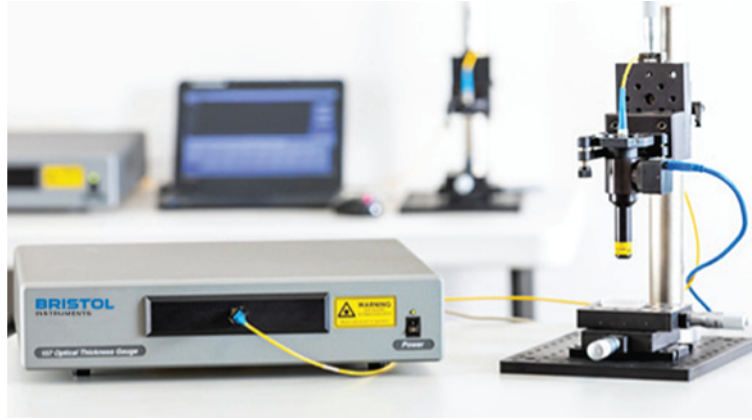


Figure 4.4: Bristol Optical Thickness Gauge 157, instrument (left) and collimated output (right).

and were crossed. Parts under test were placed on a stage between the crossed polarizers, and were rotated until extinction was observed. At the extinction position, thickness measurements were recorded using both the ordinary and extraordinary refractive index, and then the sample under test was rotated 90° , and the measurements repeated. This test method produces four thickness measurements, of which two are approximately equal – when the optic axis of the part is parallel with the axis of the generating polarizer, the extraordinary index measurement is the true physical thickness, and when the optic axis of the part is perpendicular to the axis of the generating polarizer, the ordinary index measurement is the true physical thickness. Since this method requires knowledge of the group index of the sample under test, it is problematic if a part has an unknown index, or is of an unknown material.

This test method was verified by building a cavity – multiple Zerodur plates were optically contacted in a stepped fashion to create an air space that would vary minimally, as Zerodur has a minimal coefficient of thermal expansion ($0 \pm 0.1 \times 10^{-6}$). The spacing of the air gap was measured with the optical thickness gauge, and then parts were inserted into the cavity using a spacer, to allow the physical thickness of the air gap both above and below the part to be measured.

As the cavity had been measured previously, this allowed the physical thickness

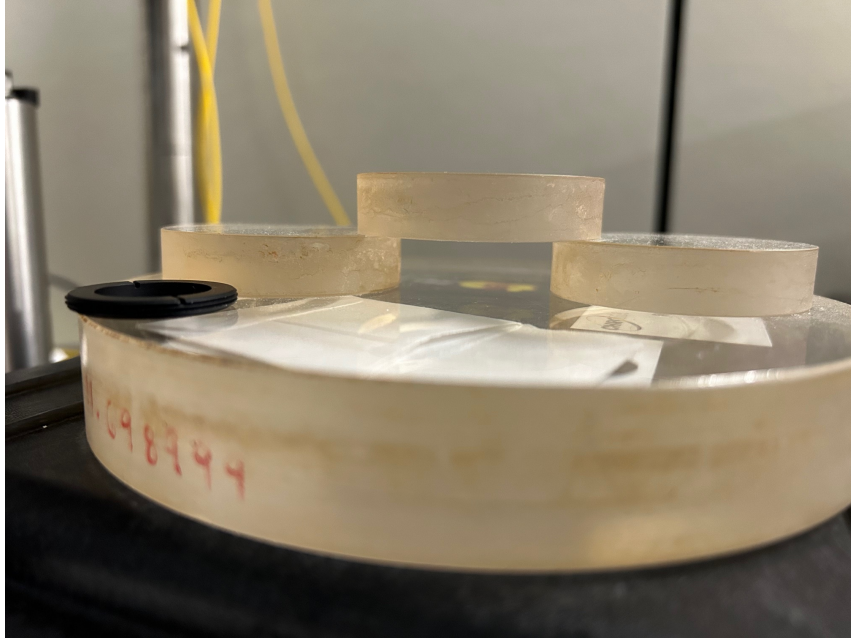


Figure 4.5: Absolute physical thickness of samples under test is measured with a Zerodur optical cavity. The 12.7 mm air space and contacted plates are shown here.

of the part placed in the cavity to be determined with a high degree of precision.

Since the cavity method allows the determination of exact physical thickness, it allows group indices of existing materials to be adjusted to the correct value, allowing measurements to be taken without using the cavity method repeatedly. This is accomplished by measuring a part of a known material using the cavity method, and then measuring the same part using the previously described crossed polarizer method, and adjusting the group index used in the crossed polarizer method until the two measurements are equal. This method had been used previously to determine the group indices for all three materials tested in this work.

4.4 Temperature Measurement

In order to compare retardance measurements taken at different temperatures, it is necessary to determine the change in retardance with temperature of the three materials with which we are concerned. While dn/dT is documented for both ordinary and extraordinary refractive indices in the literature for all three materials studied

in this work [11, 28, 25, 13, 29], as is the coefficient of thermal expansion [11, 28, 25], $d\beta/dT$ has been less reported on; when reported, it has not been measured directly, rather than reported as the difference of $dn_e/dT-dn_o/dT$, which had been measured separately [11, 25].

While birefringence changes with temperature, the crystals in this work will also expand with an increase in temperature (and consequently contract with a decrease), due to having a positive coefficient of thermal expansion. This introduces some difficulty in measuring $d\beta/dT$ directly, as both retardance and thickness change with temperature. In order to address this issue, rather than report $d\beta/dT$, there is work in the literature [12] that reports γ , which is the normalized change in retardance with temperature. This eliminates the aforementioned difficulty of both birefringence and thickness changing with temperature, as it allows the change in birefringence and physical thickness to be evaluated via one parameter. The equation for γ is given in the previously referenced work [12]

$$\gamma = \frac{1}{\delta} \frac{d\delta}{dT} = \frac{1}{\beta} \frac{d\beta}{dT} + \frac{1}{t} \frac{dt}{dT}. \quad (4.2)$$

Here, δ is the retardance, β is the birefringence, t is the physical thickness, and the Leibniz notation is the derivative of each parameter with respect to temperature.

In order to measure the change in retardance with temperature, a quartz plate in the A-plate configuration was placed in a Thorlabs heated lens tube (Thorlabs SM1L10HR), and was attached to a temperature controller. The lens tube was placed between the heads of the AxoScan polarimeter previously described, and retardance was measured from room temperature (roughly 22-25° C, depending on when and where the measurement was taken) to approximately 45° C, in roughly 2.5-5° C steps. Once the measurement was recorded at one temperature, the controller of the heated lens tube was set to the next temperature, and the waveplate was allowed to stabilize to the set temperature before the measurement was recorded. This was determined by monitoring the retardance measurement in real-time, and recording the measurement when the retardance variation over the previous two minutes was $<0.2^\circ$ of retardance ($\lambda/1800$). These measurements were averaged over

Material	Quartz	MgF ₂	Sapphire
Physical thickness	3.1560mm	1.8707mm	3.1964mm

Table 4.3: Thicknesses of parts tested for γ and $d\beta/dT$.

the aforementioned two minutes. Measurements were taken using a HeNe laser emitting at 632.8 nm. The above procedure was then repeated for magnesium fluoride and for sapphire.

The thickness of the parts tested are shown in Table 4.3. In order to maximize the change in retardance with temperature, the thickest available parts were selected.

Following the measurements being recorded, the data taken for each material were plotted in a retardance versus temperature curve. A linear trendline was fit for each material. R^2 values for each trendline can be found in Table A.14. Quartz and sapphire showed R^2 values of 0.998 or above, while MgF₂ had a lower value of 0.991. A possible reason for this would be significantly lower thickness for the MgF₂ part measured, compared to the thicknesses of the other parts tested (reported in Table 4.3), as well as a lower value of γ for MgF₂ compared to the other two materials. The value of this parameter (which is related to $d\beta/dT$) is reported in the literature [12], and the findings in this work support that MgF₂ has a lower value of γ than the other two materials studied in this work.

Linear trendlines have the general form, $y = mx + b$, where m denotes the slope of the curve. Since the slope denotes $d\delta/dT$, γ can be calculated by normalizing the retardance – by dividing the slope of the linear fit by the retardance. Additionally, $d\beta/dT$ can be extracted from the γ calculation, as Eq. 4.2 can be manipulated to

$$\frac{d\beta}{dT} = \beta \left(\gamma - \frac{1}{t} \frac{dt}{dT} \right). \quad (4.3)$$

This equation allows calculation of $d\beta/dT$, once γ has been calculated, and as long as physical thickness, birefringence at the wavelength of interest, and CTE of the material in question is known.

CHAPTER 5

Experimental Results

5.1 Spectrophotometer Results

The transmission extrema of the spectrophotometer scan of quartz from 320-860 nm (shown in Figure 4.1) are cataloged in their entirety in Table A.4, and compared to the values in waves with the data in the literature [4]. The values from the literature are calculated from the birefringence in that work, as well as the measured physical thickness of the sample. The maximum difference between the data determined by the extrema and the data in the literature is 0.011 waves. However, many of the extrema show significantly closer agreement – more than a third are within $<\lambda/500$, and the median difference is $<\lambda/250$.

From these extrema, birefringence at each wavelength in the table was calculated. The birefringence was squared and plotted against wavelength, and a curve was fit to the data using the SciPy package in Python. These data were adjusted to 20° C, (68° F) prior to being fit to a curve, to facilitate comparison to both data in the literature, as well as data across different materials. The curve used was of the form of a Sellmeier-type equation

$$\beta = \sqrt{\frac{A\lambda^2}{\lambda^2 - B} + \frac{C\lambda^2}{\lambda^2 - D} + \frac{E\lambda^2}{\lambda^2 - F}} + G. \quad (5.1)$$

The wavelength for the dispersion formula is in μm , as it is for the other dispersion formulae in this work. The values of the constants are shown in Table 5.1.

$A \times 10^4$	$B \times 10^2$	$C \times 10^3$	$D \times 10^{-2}$	$E \times 10^3$	$F \times 10^{-2}$	$G \times 10^5$
1.01599	1.92968	2.534	-1.67765	1.7741	1.000445	-2.362

Table 5.1: Quartz dispersion coefficients based on spectrophotometer data, fit to a Sellmeier-type equation, as shown in Eq. 5.1.

The data was also fit to a curve of a polynomial form to allow comparison with the Sellmeier-type equation

$$\beta = \frac{A}{\lambda^6} + \frac{B}{\lambda^5} + \frac{C}{\lambda^4} + \frac{D}{\lambda^3} + \frac{E}{\lambda^2} + \frac{F}{\lambda} + G. \quad (5.2)$$

The coefficients are shown in Table 5.2. Curve fitting using this equation has been previously reported for all three materials [30].

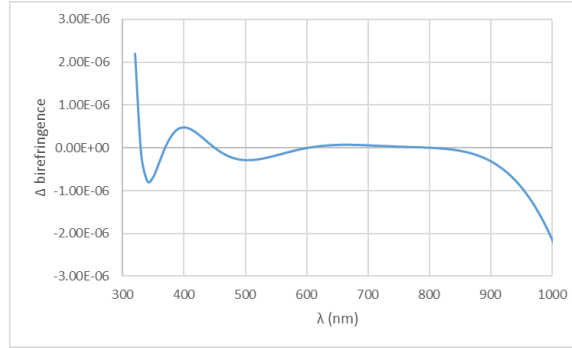
The values calculated by these two dispersion formulas (Eq. 5.1 and Eq. 5.2) with different forms are within $<3 \times 10^{-6}$ from 320 nm past 1220 nm, although the data they are calculated from ends at 860 nm. A comparison of these curves is shown in Figure 5.1a. The difference between the data in the literature and the data calculated using both dispersion formulae can also be seen in Figure 5.1b. Although the data for quartz taken via the spectrophotometer method was over the wavelength range of 320-860 nm, it shows agreement with the data in the literature [4] over a much broader range than that; there is a difference of $<1.0 \times 10^{-5}$ over the range of 320-1050 nm, nearly an additional 200 nm beyond where the data was collected in this work. (There is significant increase in the slope of the difference after 750 nm.)

As can be seen in Figure 5.1a, there is minimal (on the order of $<1.0 \times 10^{-6}$) difference between the Sellmeier-type fit and the polynomial trendline fit over the range where data was taken (320-860 nm). However, as is shown in Figure 5.1b, the polynomial data provides a closer fit to the data in the literature over a longer range, remaining within $<2.0 \times 10^{-5}$ past 1720 nm, even though the data was only taken to 860 nm, albeit with a change in slope and significant deviation from the data in the literature. This closer match is likely due to the greater number of terms in the polynomial fit.

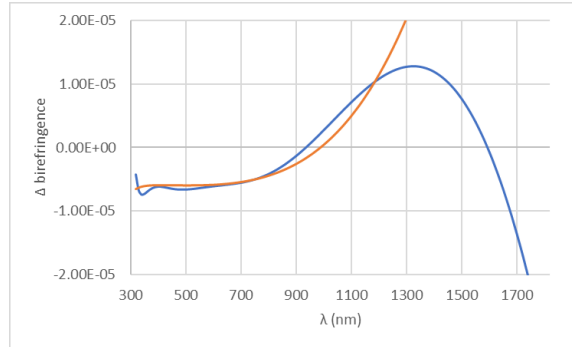
Additionally, the data taken in the ultraviolet and lower visible wavelength region

$A \times 10^5$	$B \times 10^4$	$C \times 10^3$	$D \times 10^3$	$E \times 10^3$	$F \times 10^3$	$G \times 10^3$
-1.93794	2.5197	-1.35332	3.88184	-6.20082	5.6256	6.59128

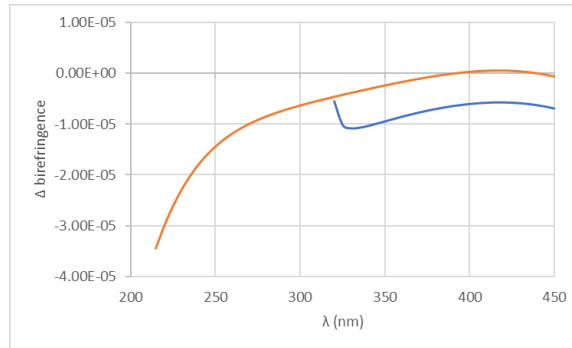
Table 5.2: Coefficients of quartz based on spectrophotometer data fit to Eq. 5.2.



(a) Birefringence difference of Sellmeier-type (Eq. 5.1, Table 5.1) and polynomial fit (Eq. 5.2, Table 5.2).



(b) Birefringence difference of literature [4] and Sellmeier-type fit (orange) and polynomial fit (blue).



(c) Birefringence difference of data taken in UV (210-450 nm, Eq. 5.1, Table 5.3) using spectrophotometer method, and data in the literature (orange curve), and difference between data from 210-450 nm and 320-860 nm (blue curve).

Figure 5.1: Quartz spectral birefringence difference from the spectrophotometer method. In (a) the difference between fitted equations is on the order of 1.0×10^{-6} over the wavelength range of 320-860 nm. In (b) is shown a comparison of the Sellmeier-type fit and the polynomial fit to the data in the literature [4]. In (c), the orange curve represents the difference between data taken from 210-450 nm and fit to a Sellmeier-type equation and the data in the literature[4], and the blue curve is the difference between the data taken from 210-450 nm and the data taken from 320-860 nm and fit to a Sellmeier-type equation (Eq. 5.1).

were fit to a curve, again using an equation of the Sellmeier-type form seen in Eq. 5.1. These data were taken from 210-450 nm, and were also adjusted to 20° C to facilitate comparison to the previously taken data, as well as to the literature. A comparison between the data taken in this region, the data taken from 320-860 nm, and the data in the literature [4] is shown in Figure 5.1c. The data taken over this wavelength range shows an increasing deviation from the data in the literature with decreasing wavelength, although the difference is $<5.0 \times 10^{-6}$ for 320-450 nm. The other data taken in this work, from 320-860 nm, shows a difference of approximately twice that, with the majority of the data showing a difference of $<1.0 \times 10^{-5}$ for 320-450 nm from the data taken deeper in the ultraviolet. The constants of the dispersion formula covering the wavelength range of 210-450 nm are shown in Table 5.3.

Magnesium fluoride was also scanned in the spectrophotometer, over a wavelength range of 300-1800 nm using the methods described previously, and had a dispersion formula fit to the peaks and troughs produced, again using the methods noted previously. The dispersion formula was, as with quartz, of the form in Eq. 5.1. The values of the constants of the dispersion formula for MgF_2 are shown in Table 5.4.

The data for MgF_2 has also been adjusted to 20° C, (68° F), as with quartz and sapphire, to facilitate comparison to both data in the literature, as well as data across different materials. When comparing the MgF_2 data taken in this work with that in the literature [5], the data in the literature has been adjusted to 20° C, using the value of $d\beta/dT$ calculated in this work, as that data had been nominally taken around 19° C [5].

As with quartz, the MgF_2 data was also fit to a polynomial trendline of the form shown in Eq. 5.2. The values of the constants used for this trendline are shown in

$A \times 10^4$	$B \times 10^2$	$C \times 10^1$	$D \times 10^{-1}$	$E \times 10^1$	$F \times 10^{-1}$	$G \times 10^5$
1.2185	1.7263	1.06977	-6.3174	1.677	9.99917	-4.6692

Table 5.3: Quartz dispersion coefficients based on spectrophotometer data in the ultraviolet and lower visible range; fit to Eq. 5.1.

Table 5.5.

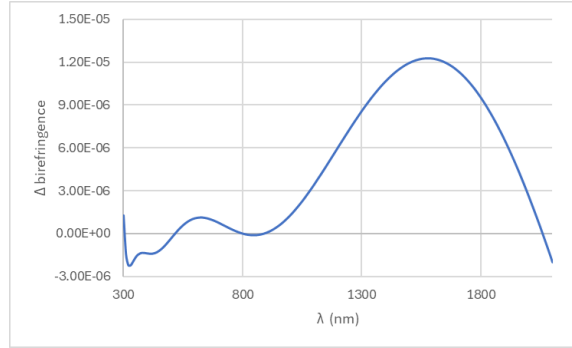
The difference between the two fits for MgF_2 is shown in Figure 5.2a. As with the comparison between the fits for quartz, there is agreement on the order of $<3.0 \times 10^{-6}$ for a significant portion of the wavelength range (approximately 300-1000 nm), but unlike the quartz comparison, there is deviation $>1.0 \times 10^{-5}$ over the wavelength range where the data was measured (300-1800 nm for MgF_2). This deviation is likely due to the different forms of the equations used (Eq. 5.1 and Eq. 5.2).

Additionally, the difference between the data in the literature [5], the data fit to the Sellmeier-type equation, and the polynomial trendline is also shown in Figure 5.2b. Much like the data taken with quartz, the polynomial trendline hews closer to the data in the literature for a longer wavelength range. However, both deviate $>1.0 \times 10^{-5}$ with respect to the data in the literature over the wavelength range over which the data was taken (300-1800 nm).

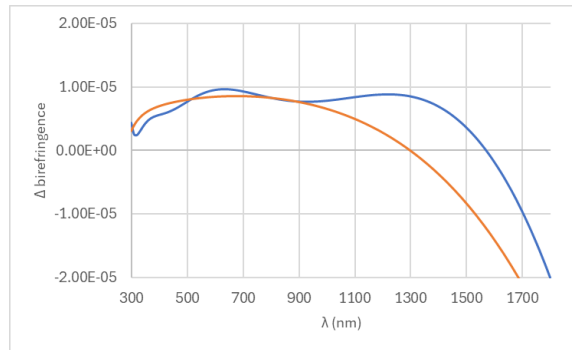
Data was also taken using the spectrophotometer method in the ultraviolet and lower visible region, from 210-450 nm. These data were fit to Eq. 5.1, and the coefficients are reported in Table 5.6. The difference between this data and the data taken previously with the spectrophotometer method, as well as the data in the literature, is shown in Figure 5.2c. The magnitude of the differences ranges from $>1.0 \times 10^{-5}$ to $<5.0 \times 10^{-6}$ for the comparison with the other data taken using the spectrophotometer, to $<2.0 \times 10^{-5}$ for the data taken in the ultraviolet to the data shown in the literature [5]. However, the difference between the data taken over the range of 300-1800 nm has a maximum difference between the data taken in the UV at 300 nm, and steadily decreases to a minimum of $>4.0 \times 10^{-6}$ around 400 nm, before increasing until the end of the wavelength range. The data taken

$A \times 10^4$	$B \times 10^3$	$C \times 10^2$	$D \times 10^{-2}$	$E \times 10^2$	$F \times 10^{-2}$	$G \times 10^4$
2.8414	5.8775	5.08832	1.02193	-4.955	1.00	-1.489

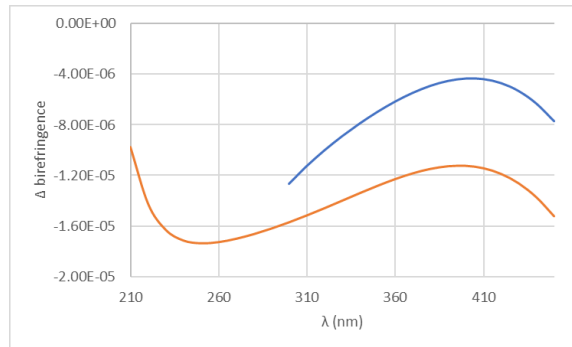
Table 5.4: MgF_2 dispersion coefficients based on spectrophotometer data, fit to Eq. 5.1.



(a) Difference between birefringence calculated using the Sellmeier-type equation (Eq. 5.1, Table 5.4) and the polynomial trendline (Eq. 5.2, Table 5.5) for MgF_2 .



(b) Difference between birefringence from the literature [5], and calculated using the Sellmeier-type equation (orange curve) and the polynomial trendline (blue curve) for MgF_2 .



(c) Difference between dispersion formula for the ultraviolet (Eq. 5.1, Table 5.6), dispersion formula calculated from 300-1800 nm (blue curve), and data in the literature (orange curve).

Figure 5.2: MgF_2 spectral birefringence difference from the spectrophotometer method. In (a) is the difference between the Sellmeier-type formula (Eq. 5.1) and the polynomial trendline (Eq. 5.2). The fits show a difference of $<3.0 \times 10^{-6}$ from 300-1000 nm. A comparison to the literature [5] for both Sellmeier-type and polynomial equations is shown in (b). Both equations show a difference of $<1.0 \times 10^{-5}$ from 300-1500 nm. Additionally, data were taken in the ultraviolet from 210-450 nm. In (c) these data were compared to both the literature [5] (orange curve), and the data taken from 300-1800 nm (blue curve).

$A \times 10^5$	$B \times 10^4$	$C \times 10^4$	$D \times 10^3$	$E \times 10^3$	$F \times 10^3$	$G \times 10^2$
-1.161	1.5618	-8.619	2.50634	-4.0046	3.58319	1.0230667

Table 5.5: MgF_2 dispersion coefficients based on spectrophotometer data fit to Eq. 5.2.

$A \times 10^3$	$B \times 10^4$	$C \times 10^{-2}$	$D \times 10^{-6}$	$E \times 10^4$	$F \times 10^0$	$G \times 10^3$
4.097303	4.8531	-2.21206	1.002246	5.5643	2.89929	-3.966994

Table 5.6: MgF_2 dispersion coefficients based on spectrophotometer data in the ultraviolet and lower visible range fit to Eq. 5.1.

from 210-450 nm does not show an increase in deviation from the literature with a decrease in wavelength.

The transmission function of a sapphire sample was also measured using the spectrophotometer method. The measurement was performed over the wavelength range of 300-1400nm, and a dispersion formula was fit to the peaks and troughs produced. The dispersion formula was similar to Eq. 5.1 but includes a negative sign prior to the square root. This negation is necessary because sapphire is a negative crystal (that is, $n_o > n_e$), and consequently the birefringence is negative. The values of the constants of the dispersion formula for sapphire have values that are shown in Table 5.7.

$$\beta = -\sqrt{\frac{A\lambda^2}{\lambda^2 - B} + \frac{C\lambda^2}{\lambda^2 - D} + \frac{E\lambda^2}{\lambda^2 - F}} + G \quad (5.3)$$

These data have likewise been adjusted, as with the other materials, to 20° C to facilitate comparison across different materials and methods, as well as the existing literature. The data were also fit to a polynomial trendline of the form in Eq. 5.2. (As the trendline is not under a square root, it does not need to be negated, in

$A \times 10^4$	$B \times 10^2$	$C \times 10^0$	$D \times 10^{-6}$	$E \times 10^5$	$F \times 10^{-1}$	$G \times 10^5$
1.02273	1.5725895	-3.64769661	3.837828326	6.810222	6.5398517	-4.135643

Table 5.7: Sapphire dispersion coefficients based on spectrophotometer data, fit to Eq. 5.3.

$A \times 10^7$	$B \times 10^6$	$C \times 10^5$	$D \times 10^5$	$E \times 10^5$	$F \times 10^5$	$G \times 10^3$
-6.7285	6.61154	-2.353	2.288	-7.167	-7.918	-7.7613

Table 5.8: Sapphire dispersion coefficients based on spectrophotometer fit to Eq. 5.2.

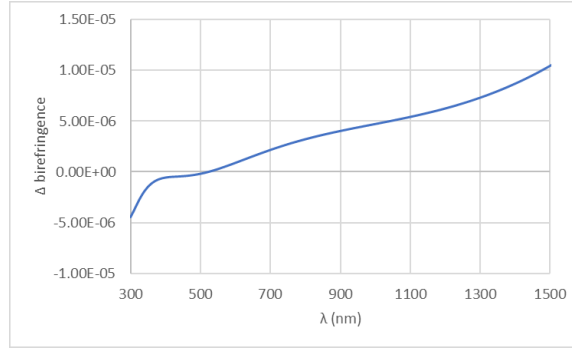
contrast to the Sellmeier-type equation used for sapphire). The difference between the trendline and the Sellmeier-type equation is shown in Figure 5.3a. The constants for the trendline are shown in Table 5.8. The difference between the two trendlines and the data in the literature for sapphire is shown in Figure 5.3b.

As with the other materials, there was additional data collected in the UV and the lower visible region from 210-450 nm. These data were fit to a Sellmeier-type equation of the form shown in Eq. 5.3. The values of the coefficients are shown in Table 5.9. A comparison of the data taken in the UV region is shown in Figure 5.3c, showing the differences between the two sets of data taken with the spectrophotometer over the UV and lower visible region, as well as the difference between the data taken in the ultraviolet and in the dispersion formula in the literature [6]. The data taken over the UV range corresponds with the data in the literature within $<1.5 \times 10^{-5}$ from 210-310 nm, and approaches the difference shown between the data taken over 300-1400 nm past that. The difference between the data taken exclusively in the UV/visible range and that of 300-1400 nm is $<1.25 \times 10^{-5}$ from 320-450 nm.

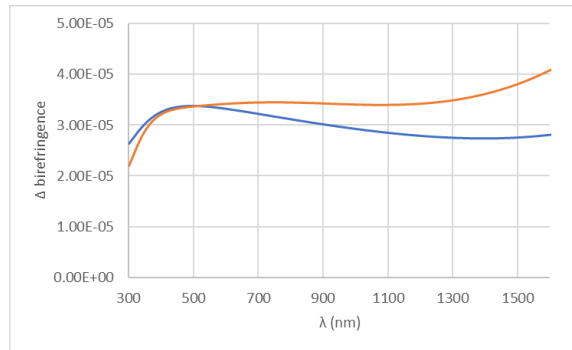
While both quartz and magnesium fluoride showed differences of approximately 1.0×10^{-5} between the data taken using the spectrophotometer method and the data in the literature, sapphire showed a difference of roughly three times that – on the order of 3.0×10^{-5} across the wavelength range where data was collected. There are a number of possible explanations for this variance between the materials: the first

$A \times 10^4$	$B \times 10^2$	$C \times 10^0$	$D \times 10^{-3}$	$E \times 10^1$	$F \times 10^{-1}$	$G \times 10^4$
1.6019	1.16892	-8.0478	1.022837	7.7958	9.9474	-1.04

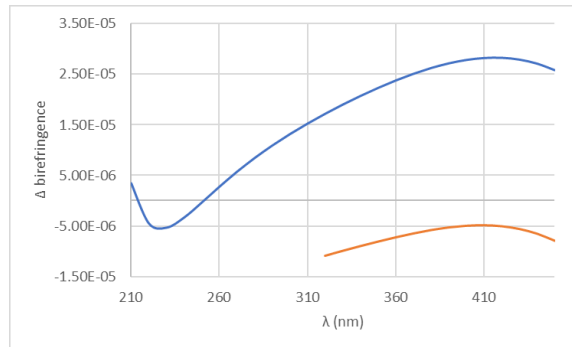
Table 5.9: Sapphire dispersion coefficients in UV based on spectrophotometer fit to Eq. 5.3.



(a) Difference between birefringence calculated using the Sellmeier-type equation (Eq. 5.3, Table 5.7) and the polynomial trendline (Eq. 5.2, Table 5.8) for sapphire.



(b) Difference between birefringence from the literature [6], and calculated using the Sellmeier-type equation (orange curve) and the polynomial trendline (blue curve) for sapphire.



(c) Difference between dispersion formula for the ultraviolet (Eq. 5.3, Table 5.9), dispersion formula calculated from 300-1400 nm (orange curve), and data in the literature (blue curve) for sapphire.

Figure 5.3: Sapphire spectral birefringence difference from spectrophotometer method. Comparison of the fit to the Sellmeier-type equation and the polynomial trendline is shown in (a), the difference between the data in the literature [6] and the two fits is shown in (b). In (c) is shown the difference between the data taken from 210-450 nm and the data taken from 300-1400 nm, and the difference between the data taken from 210-450 nm and the data in the literature [6].

is that the samples used in this work and in the literature were possibly grown using different techniques – the sapphire used in this work was exclusively grown by the Kyropoulos method, and the sapphire used in the work in the literature may have been grown by the Verneuil method, given the time period, and the history of crystal growth in the United States [31]. As crystals grown by different methods can have different refractive indices (as shown in other works in the literature [29]), variation of values of birefringence between different growth methods may be possible.

A second possibility as to why there is a larger difference shown between the measured data in this work and the data in the literature would be a difference in orientation of the optic axis of the sample under test – unlike this work, the data in the literature were collected via the minimum deviation method, which is a common procedure used to test refractive index [14]. Given that sapphire is a birefringent material, the optic axis would have to be oriented in the plane of the input and output faces of the prism, and perpendicular to the ground faces. Any misorientation of the optic axis with respect to the faces of the prism could result in a different measured value for birefringence.

An unlikely possibility is temperature differences – as noted in this work (which comports with data from the literature [25]), sapphire experiences a change in birefringence with temperature (that is, $d\beta/dT$) of approximately 1.0×10^{-6} . Therefore a change in birefringence of 3.0×10^{-5} would require a temperature shift of 30° C. As both this work and the previous work in the literature were conducted at or around room temperature, an error of this magnitude in either temperature measurement can be discounted as the cause of the discrepancy. (An error of 20° C would bring sapphire in line with the other materials in this work, but would still be implausible.)

5.2 Polarimeter Results

The wavelengths and the birefringence values for quartz obtained via testing with the AxoScan and the PAX polarimeter are shown in Table A.5. Wavelengths and birefringence values are averaged across three data points at each wavelength tested.

A Sellmeier-type equation was fit to the data points taken for quartz shown in Table A.5. The equation was of the form shown in Eq. 5.1. The values of the constants of the dispersion formula are given in Table 5.10.

As with the data taken using the spectrophotometer method, these data were adjusted to 20° C to facilitate comparison across methods and with the existing literature as well as to the raw data. The adjustment was performed prior to fitting the curve to the data points.

A comparison to the raw data and the Sellmeier-type fit for quartz can be seen in Table A.6, and shows a maximum difference at 975 nm, of 4.0×10^{-6} . As this is the first wavelength tested after the polarimeter used was changed, there are a number of potential issues – first, the uncertainty of anti-reflection coating thickness (which is on the parts tested at 975 nm and higher wavelengths. If an incorrect value was used for that, it would produce an erroneous value of the thickness, which would lead to an incorrect calculation of birefringence), secondly, the retardance tolerance of the polarimeters themselves, third, the potential for variation in alignment between the different setups.

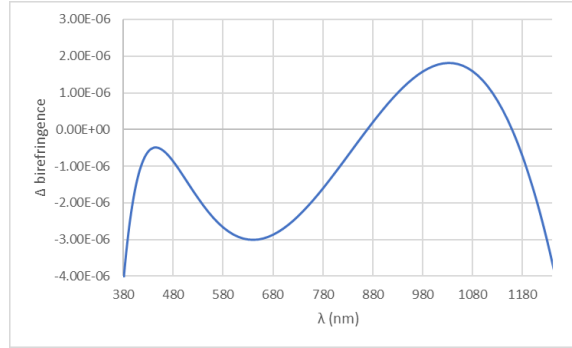
Comparison to spectrophotometer data is shown in Figure 5.4a. The two methods are within $<4.0 \times 10^{-6}$ for the value of birefringence from 380-1240 nm. Over the range where data were taken using both methods (400-860 nm), the difference is $<3.0 \times 10^{-6}$.

The difference between data taken using the polarimetric method and the existing literature [4] are shown in Figure 5.4b. The polarimeter method and the literature show a difference of birefringence within $<1.5 \times 10^{-5}$ from 400-1800 nm, with that difference being minimized to $<1.0 \times 10^{-5}$ from 400 through 1200 nm, and $<1.5 \times 10^{-5}$ for the rest of the region from 1200-1800 nm.

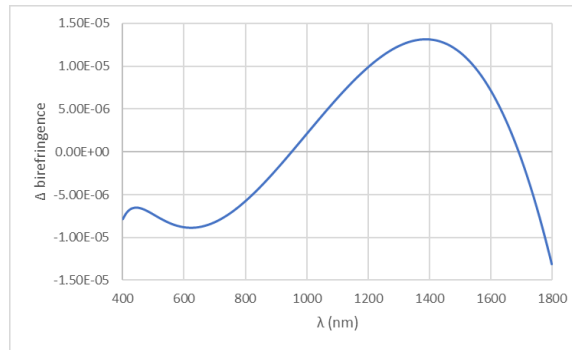
The quartz birefringence as measured with the polarimeter method was addi-

$A \times 10^5$	$B \times 10^2$	$C \times 10^0$	$D \times 10^{-4}$	$E \times 10^1$	$F \times 10^{-3}$	$G \times 10^5$
6.4724	2.719	5.26145	-1.20846	-6.694	-1.52385	1.4163

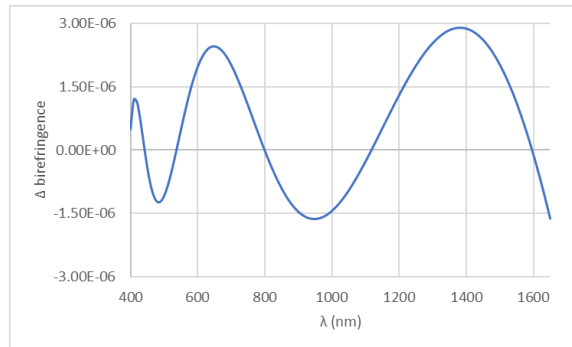
Table 5.10: Quartz dispersion coefficients based on polarimeter data fit to Eq. 5.1.



(a) Difference between birefringence per the spectrophotometer method (Eq. 5.1, Table 5.1) and polarimeter method (Eq. 5.1, Table 5.10) for quartz.



(b) Difference between birefringence per the literature data [4] and the polarimeter method for quartz. (Eq. 5.1, Table 5.10).



(c) Difference between Sellmeier-type (Eq. 5.1, Table 5.10) and polynomial fits (Eq. 5.2, Table 5.11) for quartz data taken with polarimeter method.

Figure 5.4: Quartz spectral birefringence difference from the polarimeter method. Difference between data taken using the polarimeter method, and the spectrophotometer method (a) and the literature (b) for quartz. Additionally, the difference between the polarimeter data fit to a Sellmeier-type equation and a polynomial is shown in (c). Even fitting the same data, variation of $<3.0 \times 10^{-6}$ can be seen over the spectrum where data were measured.

$A \times 10^6$	$B \times 10^5$	$C \times 10^4$	$D \times 10^3$	$E \times 10^3$	$F \times 10^3$	$G \times 10^3$
7.7794	1.44	-5.396	2.5114	-5.049	5.2089	6.6255

Table 5.11: Quartz dispersion coefficients based on laser and polarimeter fit to Eq. 5.2.

tionally fit to a polynomial trendline of the form in Eq. 5.2. The coefficients are shown in Table 5.11.

A comparison of the Sellmeier-type equation and the polynomial trendline is shown in Figure 5.4c over the wavelength range of 400-1650 nm. Over the measured wavelength range, the difference between the two fits to the data is $<3.0 \times 10^{-6}$. The difference is periodic, due to the different types of fits used.

Magnesium fluoride was also measured using the polarimeter method. For MgF_2 , the measured wavelength and temperature adjusted birefringence values are shown in Table A.7, and a Sellmeier-type equation was fitted to those data points. The equation was of the form of Eq. 5.1. The values of the constants are shown in Table 5.12.

A comparison for MgF_2 of the measured data and the fit to a Sellmeier-type equation is shown in Table A.8. The results of the curve fit are shown in Figure 5.5, which illustrates why the fit significantly deviates from the measured data at 852.5 nm, and at the last two wavelengths measured – it does not appear that a curve can be drawn that would intersect all of the points shown. This issue may be due to measurement errors, either in the retardance, wavelength, or thickness of the samples used at longer wavelengths.

The difference in birefringence measured between the spectrophotometer method and the polarimeter method for MgF_2 are shown in Figure 5.6a. The difference between the polarimeter method and the data in the literature are shown in Fig-

$A \times 10^4$	$B \times 10^3$	$C \times 10^{-2}$	$D \times 10^{-8}$	$E \times 10^1$	$F \times 10^{-5}$	$G \times 10^5$
1.7083	9.264	1.3969	-2.535	-3.6833	-1.16222	-3.53

Table 5.12: MgF_2 dispersion coefficients based on polarimeter data fit to Eq. 5.1.

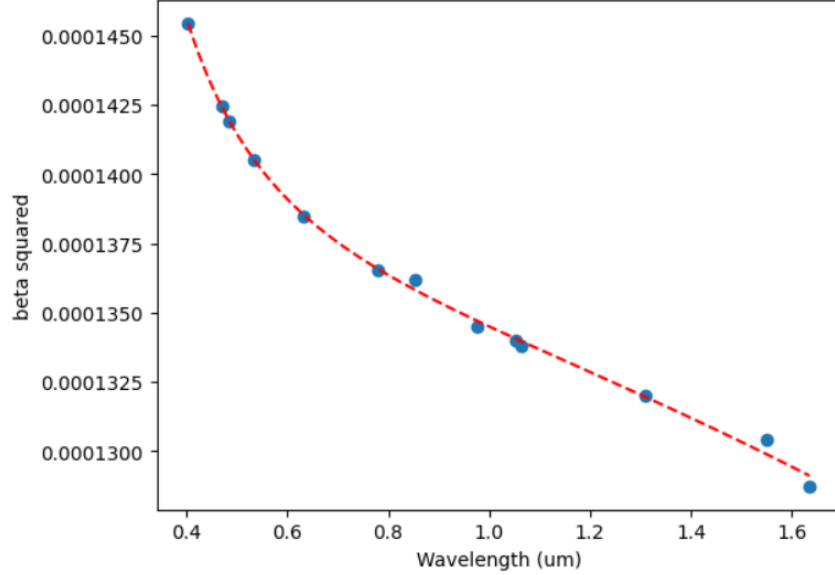


Figure 5.5: Fit of MgF₂ birefringence squared to Eq. 5.1. Notable deviations occur at 850 nm, 1549 nm, and 1636 nm. This error may be attributed to anti-reflection coating thickness and source wavelength.

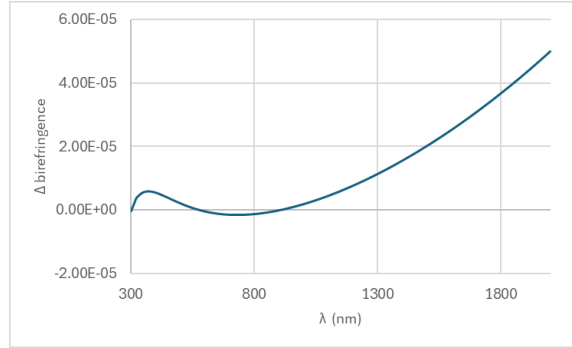
ure 5.6b. There is agreement to approximately $<1.0 \times 10^{-5}$ over the wavelength range of 300-1000 nm. The fit deviates significantly after 1000 nm, and reaches 2.5×10^{-5} around 1630 nm, which was the last wavelength measured using the polarimeter method.

The MgF₂ data taken with the polarimeter were also fit to an equation that is similar to a Sellmeier-type equation. While the form is similar to that of a Sellmeier-type equation with inverse wavelength, unlike a Sellmeier-type equation, it does not feature a square root. The coefficients for the data taken for MgF₂ using the laser sources and polarimeters and fit to Eq. 5.4 are shown in Table 5.13.

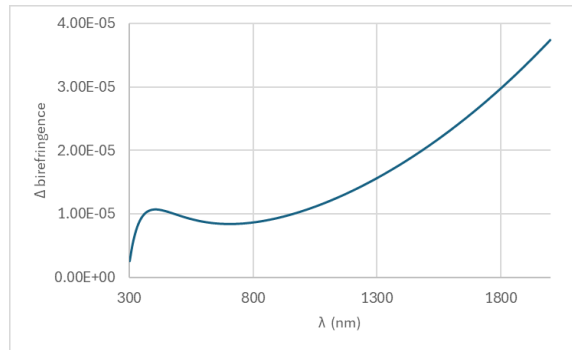
$$\beta = \frac{A(1/\lambda)^2}{(1/\lambda)^2 - B} + \frac{C(1/\lambda)^2}{(1/\lambda)^2 - D} + \frac{E(1/\lambda)^2}{(1/\lambda)^2 - F} + \frac{G(1/\lambda)^2}{(1/\lambda)^2 - H} + I. \quad (5.4)$$

A×10 ²	B×10 ³	C×10 ²	D×10 ⁻³	E×10 ⁷	F×10 ⁰	G×10 ²	H×10 ⁻²	I×10 ²
7.582315	-1.5317	-6.446	-1.1247	9.502	7	-1.67486	1.3697	-6.41754

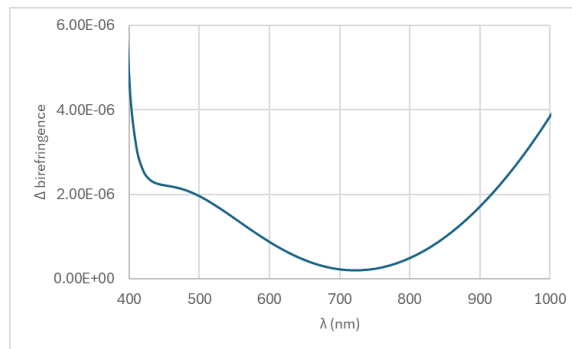
Table 5.13: MgF₂ dispersion coefficients based on laser data fit to Eq. 5.4.



(a) Difference between birefringence per the spectrophotometer method (Eq. 5.1, Table 5.4) and polarimeter method (Eq. 5.1, Table 5.12) for MgF_2 .



(b) Difference between birefringence per the literature data [5] and the polarimeter method for MgF_2 .



(c) Difference between multiple birefringence fits of different forms (Eq. 5.1, Table 5.12, Eq. 5.4, Table 5.13) for MgF_2 for data taken with the polarimeter method.

Figure 5.6: MgF_2 spectral birefringence difference from the polarimeter method. Graph (a) shows the difference between the data taken for MgF_2 using the polarimeter method (Eq. 5.1, Table 5.10) and the spectrophotometer method (Eq. 5.1, Table 5.1). The difference between the data collected using the polarimeter method and the data in the literature [5] is shown in (b). The difference between fits for data taken with the polarimeter method to an equation of the Sellmeier-type form (Eq. 5.1, Table 5.12), and an equation of the form shown in Eq. 5.4, with the coefficients in Table 5.13 is shown in (c).

The difference between the fits (that of the Sellmeier-type form and the similar equation with inverse wavelength) is shown in Figure 5.6c. There is agreement $<5.0 \times 10^{-6}$ from 400-1000 nm between the two fits. In general, the data taken for MgF_2 with the polarimeter does not agree with the data in previous work [5] better than $<1.0 \times 10^{-5}$, except over relatively brief stretches, as the data taken in this work appears to be offset from the data recorded in Dodge by approximately that amount.

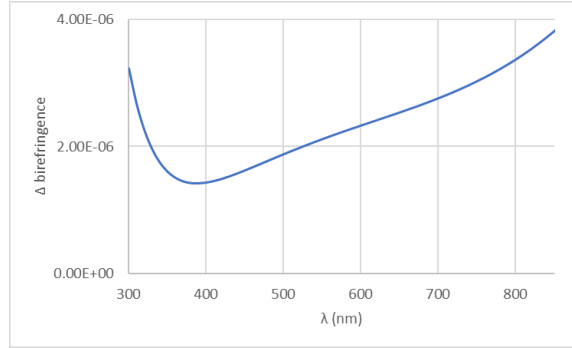
Sapphire was not measured on the PAX polarimeter, and was measured on the AxoScan polarimeter only. The measured wavelengths and temperature adjusted values of birefringence are shown in Table A.9, and a Sellmeier-type equation was fitted to those data points. The equation was of the form used previously, as shown in Eq. 5.3. The values of the constants are shown in Table 5.14.

A comparison of the measured data for sapphire to the Sellmeier-type fit is shown in Table A.10. All values are within $<1.0 \times 10^{-6}$, and the data at the majority of the wavelengths have a fit of better than $<5.0 \times 10^{-7}$. The reason for sapphire having a better agreement between the fit and the measured data compared to the other materials studied is likely due to the shortened wavelength range over which it was measured, the measurement of uncoated parts removing potential ambiguities about coating thickness, and use of the AxoScan setup avoiding potential alignment issues with the PAX polarimeter.

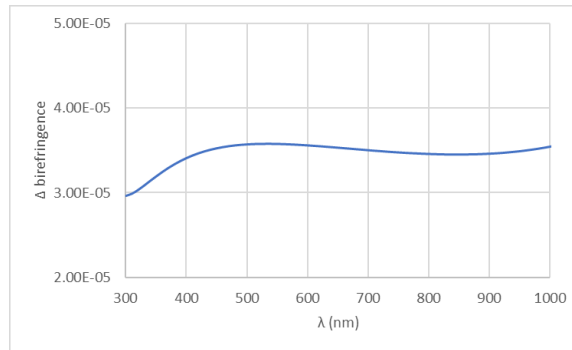
The difference between the spectrophotometer method and the polarimeter method for sapphire is shown in Figure 5.7a. The difference between the polarimeter method and the data in the literature is shown in Figure 5.7b. The data taken with the polarimeter method was also fit to a polynomial of the format in Eq. 5.2. The coefficients of the equation are shown in Table 5.15. The difference between the Sellmeier-type equation and the polynomial trendline fit are also shown in Fig-

$A \times 10^5$	$B \times 10^2$	$C \times 10^5$	$D \times 10^0$	$E \times 10^6$	$F \times 10^0$	$G \times 10^5$
9.734415	1.6354	-7.26744	-8.12124	-4.92746	7.295399	-3.63199

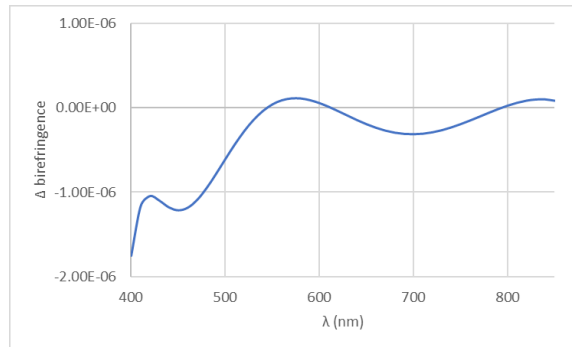
Table 5.14: Sapphire dispersion coefficients (Eq. 5.3) based on polarimeter data.



(a) Difference between birefringence per the spectrophotometer method (Eq. 5.3, Table 5.7) and polarimeter method (Eq. 5.3, Table 5.14) for sapphire.



(b) Difference between birefringence per the polarimeter method and the data in the literature [6] for sapphire.



(c) Difference between birefringence for sapphire to polarimeter data using Sellmeier-type (Eq. 5.3, Table 5.14) and polynomial (Eq. 5.2, Table 5.15) fits.

Figure 5.7: Sapphire spectral birefringence difference from the polarimeter method. Difference in birefringence of sapphire between data obtained from the polarimetric method (Eq. 5.3, Table 5.14) and the spectrophotometer method (Eq. 5.3, Table 5.7) is shown in (a). Difference between the polarimeter method and the data in the literature [6] is shown in (b). Difference between birefringence for sapphire using Sellmeier-type (Eq. 5.3, Table 5.14) and polynomial fits (Eq. 5.2, Table 5.15) is shown in (c).

ure 5.7c. The fit is $<2.0 \times 10^{-6}$ for the entirety of the range, and $<5.0 \times 10^{-7}$ for 510-850 nm.

For two of the materials studied in this work (quartz and magnesium fluoride), the difference between the data obtained via the polarimeter method and the data in the literature was $<1.5 \times 10^{-5}$ over the majority of a wavelength range encompassing the data taken on the polarimeter, when comparing data fit to a Sellmeier-type equation. For sapphire, there was a greater difference, as the difference between the data in this work and that in the literature was on the order of $<3.5 \times 10^{-5}$.

Additionally, the two independent methods used agreed within $<3.0 \times 10^{-6}$ for quartz from 400-1000 nm, $<1.0 \times 10^{-5}$ for MgF_2 from 300-1250 nm, and $<4.0 \times 10^{-6}$ for sapphire from 300-850 nm (although the polarimetric method was only used from 400-850 nm for sapphire, narrowing the range of comparison to 400-850 nm does not change the fit and agreement significantly). Elevated uncertainty for MgF_2 in the NIR may be due to uncertainty in anti-reflection coating thickness leading to an error in the measurement of the thickness of the plates tested with the polarimeter method. This potential issue is illustrated in Figure 5.5, which illustrates the some of data points significantly offset from the resulting curve.

5.3 Tolerances

The previous section covers the differences between the data collected in this work and the data in the literature, as well as the differences between the data collected in this work across two separate and independent methods. In order to establish the accuracy of these comparisons, an accounting of the tolerances of the measurements must be made.

As the spectrophotometer produces a non-collimated beam, potential errors due

$A \times 10^5$	$B \times 10^4$	$C \times 10^3$	$D \times 10^3$	$E \times 10^3$	$F \times 10^3$	$G \times 10^3$
7.244	-7.78	3.4226	-7.8971	9.9657	-6.7301	-5.9604

Table 5.15: Sapphire dispersion coefficients based on polarimeter data fit to Eq. 5.2.

to the $f/\#$ of the optical system must be taken into account. There are two different effects which need to be accounted for – first, a plane parallel plate in a non-collimated converging beam has a slightly longer path length (i.e. appears to be thicker) than it is in reality [32]. Secondly, a non-collimated beam incident on a birefringent plate will experience n_{ee} rather than n_e [15], and consequently, the value of the birefringence will appear to be smaller, as n_{ee} varies from the values of n_e to n_o . At the relatively small angles of a non-collimated incident beam, n_{ee} will be slightly less than n_e (for a positive crystal) or slightly greater than n_e (for a negative crystal), therefore decreasing the magnitude of the birefringence

$$n_{ee} = \left(\frac{\cos^2\theta}{n_o^2} + \frac{\sin^2\theta}{n_e^2} \right)^{-\frac{1}{2}}. \quad (5.5)$$

These effects vary with wavelength, for obvious reasons – the effect of a plane parallel plate is related to refractive index, which changes due to dispersion, and the effective index varies with wavelength as well, as it is derived from both the ordinary and the extraordinary refractive index, both of which also experience dispersion.

The thickness of the plates used for spectrophotometer testing were previously documented in Table 4.1. In Table A.12 is shown the apparent increase in thickness due to the non-collimated beam of the spectrophotometer ($f/9.4$) [33] for each material. These differences, while seemingly small, are significant – depending on material and wavelength, they represent a change in birefringence of 3.5×10^{-6} to 1.0×10^{-5} . These values are approximately constant in the UV-VIS region of the spectrophotometer, varying slightly ($< 0.01 \mu m$) with wavelength from 320-860 nm. Table A.12 shows the average difference in apparent physical thickness for all three materials over the wavelength range of 320-860 nm in μm .

Additionally, the effect of not experiencing the full value of birefringence is quite significant. This effect is shown in Table A.13, as the value at 320 nm is $> 1 \mu m$ for MgF_2 and sapphire. At 860 nm, the value is still greater than the decrease due to a plane parallel plate for those two materials; these two materials show a significantly greater effect than quartz because the parts measured for those materials are significantly thicker, both physically and optically, than the measured quartz plate.

While these effects have opposite signs, they do not cancel each other out for the parts in question, and the effects remain similar at longer wavelengths. Table 5.16 shows the combined results of the two effects in terms of apparent increase in physical thickness of the plate in question.

These changes in effective thickness in opposite directions have an effect on the birefringence that is shown in Figure 5.8. As can be seen, this effect is significant for both quartz and MgF_2 (both on the order of 6.5×10^{-6}), while less so for sapphire.

In addition, the wavelength accuracy and resolution of the spectrophotometer must be considered. The wavelength accuracy of the instrument used is ± 0.08 nm from 175-860 nm, and ± 0.2 nm beyond 860 nm, per the instrument's manual [2]. The uncertainty in birefringence due to the wavelength accuracy of the spectrophotometer is shown in Figure 5.8b. This uncertainty varies with wavelength, decreasing from the UV through the visible until increasing at 860 nm when the detector and the grating in the instrument changes (causing the tolerance to change), and then decreasing again with increasing wavelength. Since wavelength accuracy is a symmetrical tolerance, this potential error is symmetric as well, and can be thought of as rotated about the abscissa (that is, the form of the error is \pm).

Additionally, as the temperature is adjusted to 20° C, the error in the temperature sensor must be considered. The temperature sensor used has a specified accuracy of $\pm 1.0^\circ$ F ($\pm 0.56^\circ$ C). The temperature is taken at the beginning and the end of each scan and then averaged, so the maximum possible error of the average would be $\pm 0.56^\circ$ C. The results of the change in birefringence with temperature for each material is shown in a later section, as well as in the literature [12, 25], so the error induced by an error in the temperature sensor reading would be $d\beta/dT$ as shown in Tables 5.18, 5.19, 5.20 for quartz, MgF_2 , and sapphire, respectively, mul-

	Quartz	MgF_2	Sapphire
320 nm	0.44	1.03	1.03
860 nm	0.46	1.05	1.09

Table 5.16: Total change in effective thickness of plates in spectrophotometer due to effects in Tables A.12 and A.13.

multiplied by the temperature error. The potential error induced by the temperature sensor is shown in Table 5.17.

Finally, the error in the physical thickness measurement of the parts under test must be taken into account. The tolerance on the physical thickness measurement is $\pm 0.1 \mu m$.

The overall tolerance of the measurements taken in the spectrophotometer can be understood as the values in Figure 5.8 combined to form both upper and lower bounds, with the physical thickness tolerance used to adjust the upper and lower bounds, with the temperature tolerance factored in as well. The overall tolerance is shown for all three materials in Figure 5.9.

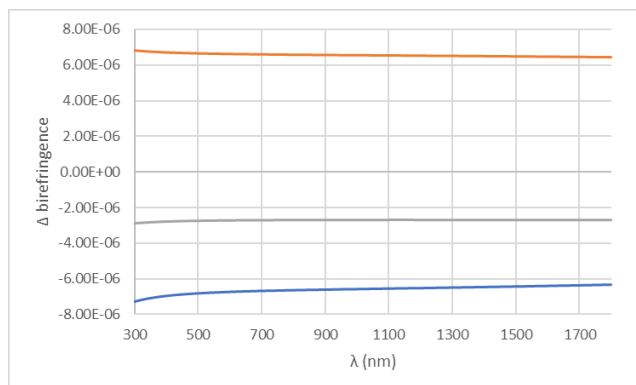
These are the error bars on data taken with the spectrophotometer method for the parts measured in this work, and are dependent on the thickness of those parts. While the repeatability of the spectrophotometer method was not evaluated in this work, the correspondence of the method across the data taken over 210-450 nm with the data taken in the visible into the NIR for all three materials, as well as the overall tolerances on the method, argue for the method being an accurate way to evaluate birefringence of a material.

The tolerances on the polarimeter method are due to the retardance accuracy of the polarimeters themselves, tolerance on the measurement of the physical thickness of the parts, tolerance on the temperature at which the measurement is taken, potential wavelength error of the laser source used, and tilt of the optic axis relative to the plane of the plate.

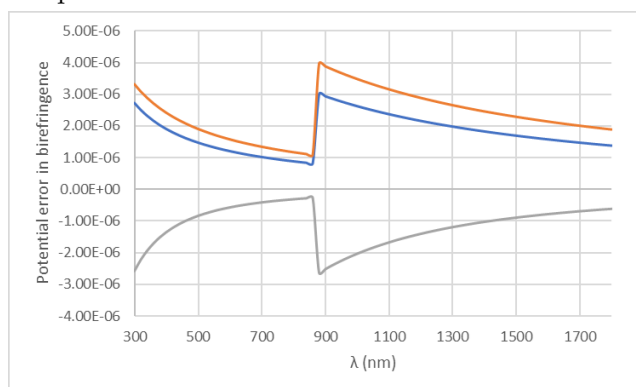
First, the retardance accuracy tolerance of the AxoScan polarimeter is specified by Axometrics as 0.2° of retardance ($\lambda/1800$), whereas the tolerance of the PAX1000IR2 polarimeter head is 0.5° of retardance ($\lambda/720$). Thorlabs specifies a tolerance of 0.25° of ellipticity ($\lambda/1440$), but ellipticity must be multiplied by 2 to

Quartz	MgF ₂	Sapphire
$\pm 5.56 \times 10^{-7}$	$\pm 3.28 \times 10^{-7}$	$\pm 5.67 \times 10^{-7}$

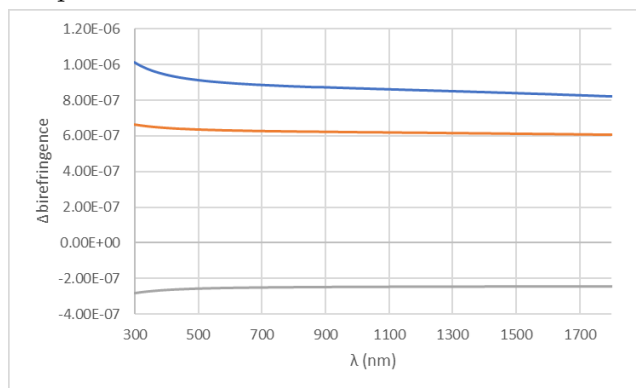
Table 5.17: Birefringence error due to potential temperature error in sensor.



(a) Potential error in birefringence due to non-collimated beam in spectrophotometer.

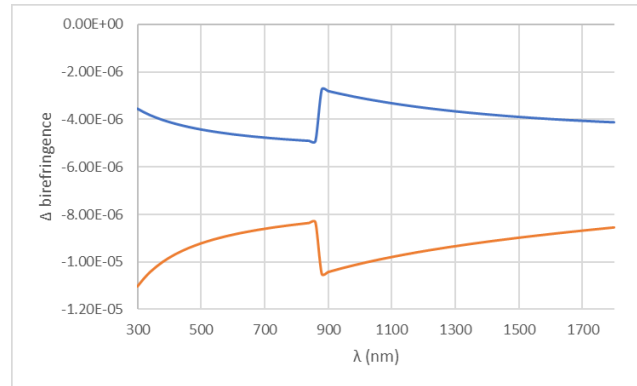


(b) Potential birefringence error due to wavelength uncertainty in spectrophotometer.

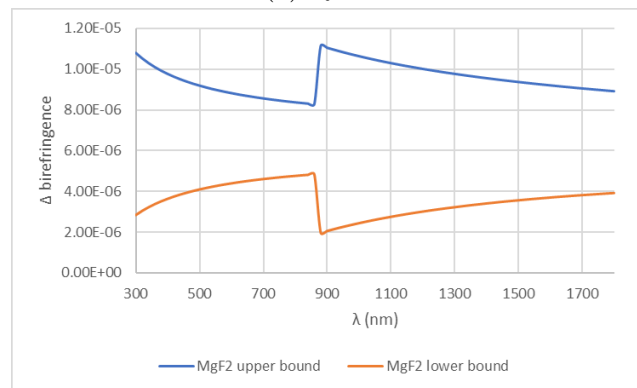
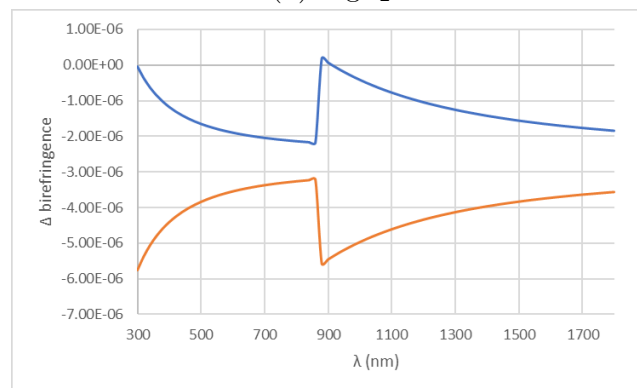


(c) Potential birefringence error due to tolerance on physical thickness of parts.

Figure 5.8: The three largest sources of uncertainty in the spectrophotometer method. In (a) is the variation of birefringence error due to dual effects of non-collimated beam versus wavelength characterized in Table 5.16. In (b) is the effect of wavelength tolerance in the instrument. Discontinuity is due to grating and detector change. Curves are shown for one sign only, but are \pm , so should be understood as rotated about the abscissa. Potential error due to physical thickness tolerance is shown in (c). Graphs are color coded: blue (quartz), orange (MgF₂), gray (sapphire).



(a) Quartz

(b) MgF₂

(c) Sapphire

Figure 5.9: Potential total birefringence error for all three materials due to uncertainty in spectrophotometer. Discontinuity is where the error changes, due to grating and detector change in the instrument. The blue curve is the upper bound of the tolerance for all three materials, and the orange curve is the lower bound.

obtain the retardance in degrees. These vary with wavelength, and are shown in Figure 5.10a. The sharp discontinuity is due to changing the polarimeter used in the NIR, with the AxoScan being used to 850 nm, and the PAX1000IR2 used at wavelengths longer than 850 nm, generally beginning at nominally 980 nm (although the source used emitted closer to 975 nm) as the PAX1000IR2 has a retardance uncertainty two-and-a-half times greater than the AxoScan.

Secondly, as detailed earlier, the tolerance of the Bristol measurement system is $\pm 0.1 \mu\text{m}$, which imparts an uncertainty in the birefringence of 9.09×10^{-7} at 632.8 nm for an approximately 1 mm thick quartz part. This uncertainty varies minimally with wavelength, as shown in Figure 5.10b. The quartz data has a non-regular shape as different parts (and hence different thicknesses) were used for each wavelength. A similar issue can be observed for the two MgF_2 datapoints farthest in the NIR, as different thicknesses were used there, as well. The sapphire data is nearly linear, as parts of the same thickness were used.

The tolerance on temperature is simply the tolerance on the temperature sensor used ($\pm 0.56^\circ \text{C}$), multiplied by $d\beta/dT$ for each material. The potential error due to temperature uncertainty is shown in Figure 5.10c. While quartz and sapphire have very similar $d\beta/dT$ s in terms of magnitude (and therefore similar potential error in birefringence), that of MgF_2 is significantly smaller, as it has a lower value of $d\beta/dT$ than the other two materials.

The tolerance on wavelength uncertainty is that of the optical spectrum analyzer used. Per Thorlabs, that is ± 2 ppm, which produces a wavelength uncertainty that is also shown in Figure 5.10d. This potential error is an order of magnitude less than the previously listed sources of error in this work.

The tolerance on the tilt of the optic axis is <6 arcmin for quartz and MgF_2 , and <12 arcmin for sapphire, per the raw material suppliers used. Tilt of the optic axis with respect to the face of the plate would produce an effect that was noted previously, in that light impinging on the part would not experience the full value of birefringence, but the difference between n_{ee} and n_o , with n_{ee} defined in Eq. 5.5. Given the relatively tight tolerance on the angles, this effect is relatively minimal,

and as also shown in Figure 5.10e, and is of a comparable magnitude to the potential error in wavelength.

The total error in the birefringence for the polarimeter and laser setup is shown in Figure 5.10f. The discontinuity observed for quartz and MgF_2 in the NIR region is due to the change in polarimeter from the AxoScan to the PAX1000IR2, as the PAX1000IR2 has a larger tolerance on retardance measurement than the AxoScan.

Additionally the total error in the polarimeter, like the error in the spectrophotometer, is \pm , so it should be understood that the error shown in Figure 5.10 should be rotated about the abscissa to show the total error range. Unlike the error in the spectrophotometer, the upper and lower bounds are symmetric about the abscissa.

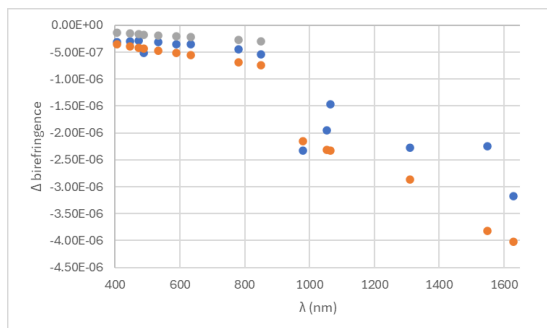
Overall tolerances are mostly dependent on physical thickness of parts used for measurement, and are $<3.0 \times 10^{-6}$ for quartz, $<3.0 \times 10^{-6}$ for MgF_2 , and $<1.5 \times 10^{-6}$ for sapphire. This discrepancy is due to the data for quartz being collected on parts ranging in thickness from 0.5-1.0 mm, MgF_2 on parts ranging from 0.5-0.8 mm in thickness, and sapphire on parts approximately 1.6 mm in thickness.

These tolerances on the value of birefringence using the polarimeter method are approximately an order of magnitude less than had been previously reported in the literature [4, 5, 6], and potentially allow a more accurate determination of birefringence for the materials studied in this work.

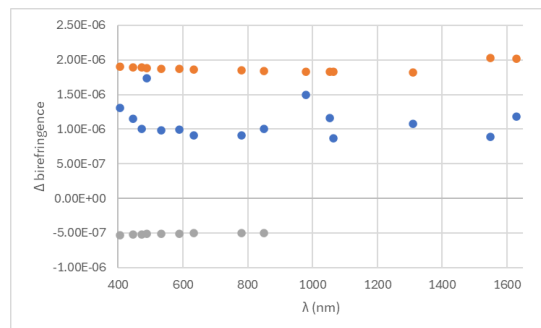
5.4 Temperature Results and Tolerances

The change in retardance with temperature are shown for each material in Figure 5.11. The temperatures samples and observed retardance are provided in Tables A.1, A.2, and Table A.3 for quartz, MgF_2 , and sapphire, respectively.

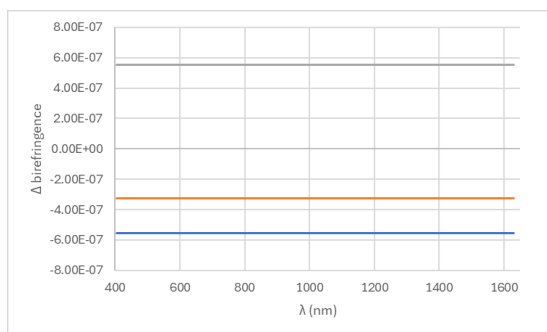
All three materials studied show a decrease in absolute retardance with increasing temperature. This indicates that $d\beta/dT$ is negative for quartz and MgF_2 , and positive for sapphire. While the sapphire has an opposing slope of the curve when compared to quartz and MgF_2 , the absolute magnitude of its retardance is also decreasing, as it is a negative crystal, and therefore its retardance is negative.



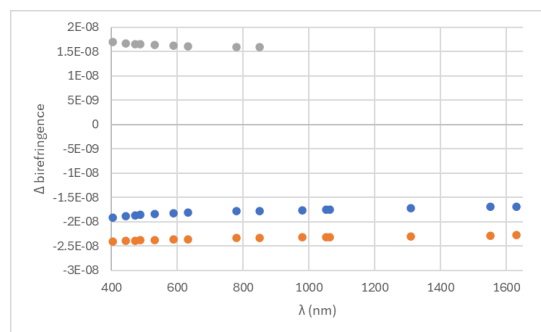
(a) Potential error due to tolerance of each polarimeter



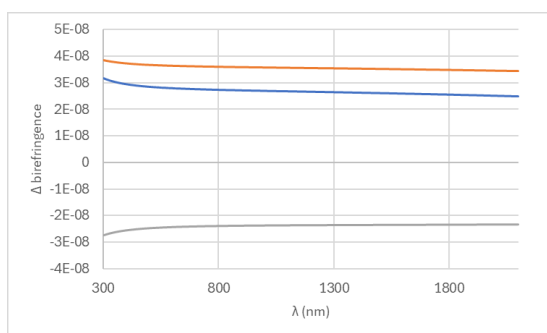
(b) Thickness of sample



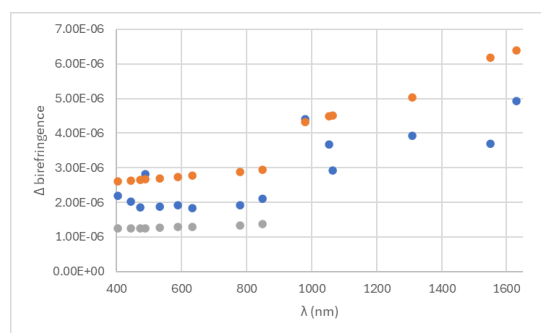
(c) Temperature sensor



(d) Wavelength uncertainty



(e) Axial tilt



(f) Total potential error in birefringence measurement. Sum of graphs a-e

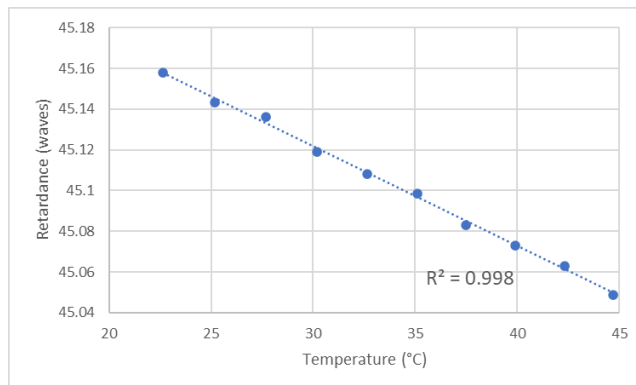
Figure 5.10: Potential sources of error for polarimeter method. Discontinuities in graphs (a) and (f) are due to change in polarimeter used. Variation in error with wavelength in graph (b) due to different thicknesses of parts being used. Graphs are color coded: MgF_2 (orange), quartz (blue), and sapphire (gray).

From these curves, both γ and $d\beta/dT$ are calculated for each material, and the results are compared to previous work in the literature. Temperatures were read out from the internal thermistor on the temperature controller, and the actual temperature did not always exactly match the set temperature. Values were typically within 0.3°C of the set temperature, as is shown in Tables A.1, A.2, and A.3 for quartz, magnesium fluoride, and sapphire, respectively.

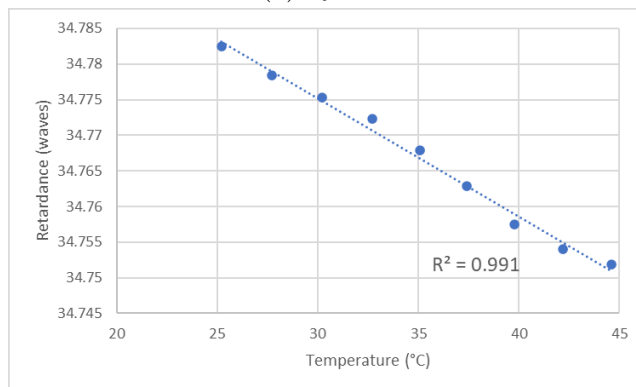
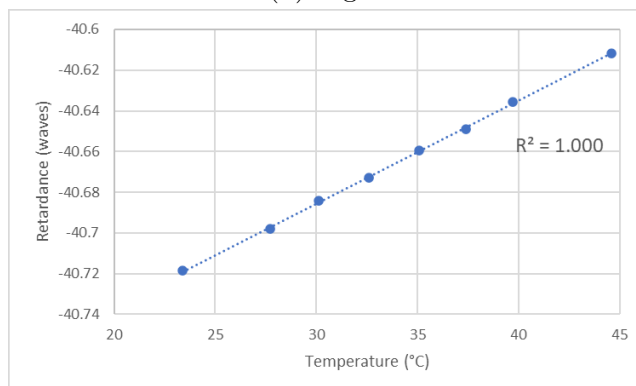
As the AxoScan polarimeter cannot trivially determine waveplate order number, the order number was calculated using existing literature at room temperature [4, 5, 6]. This approach was also used to determine whether a measurement was greater or less than a half wave, as the range of the polarimeter is from zero to $1/2$ wave. Retardances greater than a half wave wrap around (e.g. the polarimeter would record 0.75 waves as 0.25 waves).

In Table 5.18 the data collected in this work is compared to data collected previously in the literature for quartz. γ is reported in the literature [12] for both that work and for the data collected in a previous work [11]. The result obtained for γ for quartz in this work is in line with the work done in Etzel[12] when accounting for margin of error determined for this work. The value for $d\beta/dT$ in this work is also in line with the value for $d\beta/dT$ calculated here from the data provided in Etzel. (Etzel provides both thickness of the piece under test, as well as a reported value of γ , and therefore $d\beta/dT$ can be calculated using Eq. 4.3). Neither the values of $d\beta/dT$ in Toyoda [11], nor the value of γ calculated in Etzel for the data in Toyoda match the values recorded here, but given that the data was recorded at a different wavelength, and given the potential for dispersion of $d\beta/dT$, it is possible that the data taken in that work is in line with the data taken in this work. Additionally, given the error bars on the data in Toyoda reported in Etzel, the error bars on that data nearly overlap with the data taken in this work.

The tolerancing on $d\beta/dT$ and γ were calculated by determining the potential error on physical thickness, retardance, and wavelength for the parts measured, as well as temperature for the temperature controller used. The values of these potential sources of error were discussed previously.



(a) Quartz

(b) MgF₂

(c) Sapphire

Figure 5.11: Change in retardance with temperature for: (a) quartz, (b) MgF₂, and (c) sapphire. Sapphire has a positive slope because the birefringence is negative.

For quartz, the change in retardance with temperature is mostly due to the values of dn_o/dT and dn_e/dT changing at different rates, and producing $d\beta/dT$. This is because the change in temperature measured will induce an increase in physical

thickness, which, if $d\beta/dT$ were equal to zero, would produce an increase, rather than a decrease in retardance, due to quartz having a positive coefficient of thermal expansion.

For magnesium fluoride, the data in this work do not comport with the values given in the literature [12], even accounting for the margin of error determined for this work. This may be due to a significant difference in thickness in the parts used – in this work, the magnesium fluoride sample was 1.8707 mm thick, as reported in Table 4.1, whereas in the literature [12], the measured MgF_2 plate was 25.6mm in thickness. Another possible issue is the poor quality of the fit – of the three materials tested in this work, magnesium fluoride had the lowest quality of fit to the retardance versus temperature data. This may be due to the lack of thickness of the plate used ($<1.9\text{mm}$, as opposed to $>3.15\text{mm}$ for quartz and sapphire, as shown in Table 4.1), or possibly be due to the retardance of magnesium fluoride being less sensitive to change in temperature than the other materials – as is shown in Table 5.19 below, per the literature [12] as well as this work, MgF_2 has a value of γ approximately half of that reported for quartz and sapphire.

For sapphire, $d\beta/dT$ has been less reported on in the literature, as much existing work has focused on dn/dT (often of the ordinary ray, as the fact that sapphire is birefringent is not the primary driver in its use as an optical material; rather, its high durability, resistance to chemicals, insensitivity to elevated temperatures, and broad transmission window, are). However, the results here are in line with the other

	Toyoda[11]	Etzel[12]	This work
Wavelength	609.5 nm	632.8 nm	632.8 nm
$d\beta/dT$	-1.3×10^{-6}	-1.1×10^{-6}	$-1.0 \times 10^{-6} \begin{smallmatrix} +1.49 \times 10^{-7} \\ -1.00 \times 10^{-7} \end{smallmatrix}$
γ	-1.45×10^{-4}	-1.213×10^{-4}	$-1.10 \times 10^{-4} \begin{smallmatrix} +1.11 \times 10^{-5} \\ -1.64 \times 10^{-5} \end{smallmatrix}$

Table 5.18: Comparison of $d\beta/dT$ and γ for quartz in the literature and this work. Toyoda reports a value of $d\beta/dT$, whereas the value of $d\beta/dT$ for Etzel is calculated from parameters provided in that paper. Etzel does provides a value of γ from the data reported in Toyoda, and that value is reproduced here.

	Etzel[12]	Duncanson[28]	This work
Wavelength	632.8 nm	706.5 nm	632.8 nm
$d\beta/dT$	-6.6×10^{-7}	-0.9×10^{-6}	$-5.9 \times 10^{-7} \begin{smallmatrix} +1.35 \times 10^{-7} \\ -0.44 \times 10^{-7} \end{smallmatrix}$
γ	-5.55×10^{-5}	N/A	$-4.77 \times 10^{-5} \begin{smallmatrix} +8.98 \times 10^{-6} \\ -6.25 \times 10^{-6} \end{smallmatrix}$

Table 5.19: MgF_2 temperature dependence where γ cannot be computed for Duncanson, as $d\beta/dT$ for that work is calculated by the deviation from a prism, rather than a retardance measurement.

work done in the literature [25], although the wavelengths tested were significantly different. Other papers [7] have published data on different wavelengths than what is reported in this work, although the reported measurements (for γ , no measurements for $d\beta/dT$ are reported) are broadly in line with the measurements taken here, even given the margin of error reported in this work. There is additionally data reported in a third paper [29] that are of the same order of magnitude as what is reported here, although the sign is negative, as opposed to a positive sign measured in this work and other literature [25], which could indicate an error in sign.

The data taken above were used to adjust all retardance data taken in this work to their equivalent retardance at 20° C (68° F).

	Yang[25]	DeFranzo[29]	Kraemer[7]	This work
Wavelength	3.3 μm	654 nm	517 nm	632.8 nm
$d\beta/dT$	1.1×10^{-6}	-1.0×10^{-6}	N/A	$1.02 \times 10^{-6} \begin{smallmatrix} +1.27 \times 10^{-7} \\ -1.33 \times 10^{-7} \end{smallmatrix}$
γ	N/A	N/A	-1.354×10^{-4}	$-1.24 \times 10^{-4} \begin{smallmatrix} +1.48 \times 10^{-5} \\ -1.74 \times 10^{-5} \end{smallmatrix}$

Table 5.20: Comparison of $d\beta/dT$ and γ for sapphire. $d\beta/dT$ for Kraemer not reported, and cannot be calculated, as there is no quoted data in that work [7]. γ cannot be computed for Yang and DeFranzo, as $d\beta/dT$ for that work is calculated by the deviation from a prism, rather than a retardance measurement. Sapphire has $d\beta/dT$ and γ with opposing signs, as the retardance of sapphire is negative.

CHAPTER 6

Conclusions

The dispersion of the birefringence was determined for crystal quartz, magnesium fluoride, and synthetic sapphire across the UV, visible and NIR spectral regions using two distinct experimental techniques documented in Chapter 4. The obtained results were cross-referenced with each other and with literature findings, as detailed in Chapter 5. For each material and method, various dispersion formulas, including Sellmeier-type formulas, were calculated. As highlighted in the Introduction, birefringence uncertainty of $<1.0 \times 10^{-5}$ is essential for the fabrication of waveplates within acceptable tolerance levels. The two experimental measurement results used in this work were found to agree within $<1.0 \times 10^{-5}$. Specifically, disparities were $<4.0 \times 10^{-6}$ for quartz and sapphire, and $<1.0 \times 10^{-5}$ for MgF_2 . The comparisons with existing literature showed differences of $<1.5 \times 10^{-5}$ for quartz and MgF_2 . Additionally, the data obtained in this study deviated by $<3.5 \times 10^{-5}$ compared to literature values for sapphire. A possible reason for this larger disagreement could be that different crystal growth methods were used for the samples in this work than for the data previously reported.

In Section 5.4 the temperature dependent change in birefringence for each material was measured at 632.8 nm, and compared to previous works. As retardance is dependent on the physical thickness of the part measured, a normalization parameter for change in retardance with temperature, previously reported in the literature, was calculated for each material. The measured temperature dependent change in birefringence for quartz corresponds with data previously measured in the literature, within the tolerances of the measurement apparatus. The temperature results for sapphire correspond to previously measured data as well, again within the tolerances of the setup. The results for magnesium fluoride were similar to previous works, but did not entirely overlap; the difference between the measured value in

this work for $d\beta/dT$ and previously reported literature is 7×10^{-8} . Given the values of the tolerances in this work, this value could be as little as 2.6×10^{-8} , but does not entirely correspond with previous work. This discrepancy could be due to significant differences in the thickness of parts measured in both this and previous work in the literature.

A characterization protocol for birefringence measurements of other materials is supported by the agreement of the two experimental methods, as well as the existing literature, reported in this thesis. The tolerancing analysis, detailed in Chapter 5, shows that the uncertainty of these experimental methods is nearly an order of magnitude less than previous methods. Therefore, this work describes practical experimental options and considerations for birefringence characterization.

APPENDIX A

Additional Tabulated Results

Temperature °C	22.7	25.2	27.7	30.2	32.7	35.1	37.5	39.9	44.7
Retardance (waves)	45.158	45.143	45.136	45.119	45.108	45.099	45.083	45.073	45.049

Table A.1: Change in retardance for quartz part with temperature, showing measured temperature in °C and measured retardance in waves.

Temperature °C	25.2	27.7	30.2	32.7	35.1	37.4	39.8	42.2	44.6
Retardance (waves)	34.782	34.778	34.775	34.772	34.768	34.763	34.758	34.754	34.752

Table A.2: Change in retardance for magnesium fluoride part with temperature. Note significantly lower change in magnitude compared to quartz (Table A.1) and sapphire (Table A.3).

Temperature °C	23.4	27.7	30.1	32.6	35.1	37.4	39.7	44.6
Retardance (waves)	-40.719	-40.698	-40.684	-40.673	-40.659	-40.649	-40.636	-40.612

Table A.3: Change in retardance for sapphire part with temperature. Values of retardance are negative as sapphire is a negative crystal. Note similarity in terms of magnitude of change in the retardance to quartz (Table A.1).

Extremum	Type	Waves (Ghosh [4])	Waves (this work)
854.6 nm	Trough	10.502	10.5
818.1 nm	Peak	11.000	11.0
784.6 nm	Trough	11.500	11.5
753.9 nm	Peak	12.000	12.0
725.6 nm	Trough	12.500	12.5
699.5 nm	Peak	13.000	13.0
675.3 nm	Trough	13.500	13.5
653.2 nm	Peak	13.991	14.0
632.0 nm	Trough	14.498	14.5
612.7 nm	Peak	14.992	15.0
594.2 nm	Trough	15.500	15.5
577.2 nm	Peak	15.997	16.0
561.1 nm	Trough	16.499	16.5
546.1 nm	Peak	16.997	17.0
531.9 nm	Trough	17.498	17.5
518.6 nm	Peak	17.995	18.0
505.9 nm	Trough	18.497	18.5
494.0 nm	Peak	18.995	19.0
482.6 nm	Trough	19.498	19.5
472.0 nm	Peak	19.992	20.0
461.7 nm	Trough	20.497	20.5
452.1 nm	Peak	20.992	21.0
442.8 nm	Trough	21.497	21.5
434.1 nm	Peak	21.992	22.0
425.7 nm	Trough	22.494	22.5
417.7 nm	Peak	22.994	23.0
410.0 nm	Trough	23.498	23.5
402.7 nm	Peak	23.999	24.0
395.8 nm	Trough	24.492	24.5
389.1 nm	Peak	24.993	25.0
382.6 nm	Trough	25.500	25.5
376.5 nm	Peak	25.996	26.0
370.6 nm	Trough	26.496	26.5
365.0 nm	Peak	26.990	27.0
359.5 nm	Trough	27.494	27.5
354.3 nm	Peak	27.990	28.0
349.2 nm	Trough	28.495	28.5
344.4 nm	Peak	28.989	29.0
339.7 nm	Trough	29.491	29.5
335.2 nm	Peak	29.989	30.0
330.8 nm	Trough	30.494	30.5
326.6 nm	Peak	30.993	31
322.5 nm	Trough	31.499	31.5

Table A.4: Extrema of quartz measurement in spectrophotometer, with number of waves at that wavelength per the literature [4], and number of waves as determined in this work. Difference in significant figures is due to definition of extrema – a peak is exactly a full wave, and a trough is exactly a half wave.

λ (nm)	β (measured)	Polarimeter used
402.873	0.0095535	AxoScan
450.966	0.0093865	AxoScan
472.040	0.0093299	AxoScan
483.437	0.0093025	AxoScan
531.366	0.0092029	AxoScan
588.054	0.0091146	AxoScan
632.826	0.0090579	AxoScan
781.873	0.0089211	AxoScan
846.164	0.0088761	AxoScan
975.154	0.0087969	PAX
1052.470	0.0087489	PAX
1062.665	0.0087396	PAX
1309.071	0.0085984	PAX
1553.454	0.0084670	PAX
1629.055	0.0084255	PAX

Table A.5: Spectral birefringence of quartz from polarimetric measurements.

λ (nm)	β (measured)	β (Sellmeier fit)	Δ
402.873	0.0095535	0.0095544	-9×10^{-7}
450.966	0.0093865	0.0093858	7×10^{-7}
472.040	0.0093299	0.0093288	1.1×10^{-6}
483.437	0.0093025	0.0093011	1.4×10^{-6}
531.366	0.0092029	0.0092035	-6×10^{-7}
588.054	0.0091146	0.0091155	-9×10^{-7}
632.826	0.0090579	0.0090599	-2×10^{-6}
781.873	0.0089211	0.0089225	-1.4×10^{-6}
846.164	0.0088761	0.0088758	3×10^{-7}
975.154	0.0087968	0.0087928	4.0×10^{-6}
1052.470	0.0087489	0.0087469	2×10^{-6}
1062.665	0.0087396	0.0087409	-1.3×10^{-6}
1309.071	0.0085984	0.0086018	-3.4×10^{-6}
1553.454	0.0084670	0.0084667	3×10^{-7}
1629.055	0.0084255	0.0084254	1.0×10^{-7}

Table A.6: Comparison of measured birefringence with calculated birefringence from Sellmeier fit using Eq. 5.1 and Table 5.10.

λ (nm)	β (adjusted)	Polarimeter
402.732	0.012060	AxoScan
470.860	0.011934	AxoScan
483.730	0.011913	AxoScan
532.605	0.011855	AxoScan
632.836	0.011767	AxoScan
780.072	0.011685	AxoScan
852.507	0.011670	AxoScan
975.079	0.011598	PAX
1052.480	0.011575	PAX
1064.100	0.011568	PAX
1309.114	0.011489	PAX
1549.250	0.011419	PAX
1636.008	0.011346	PAX

Table A.7: Spectral birefringence of MgF_2 from polarimetric measurements.

λ (nm)	β (measured)	β (Sellmeier)	Δ
402.732	0.0120598	0.012060	-2×10^{-7}
470.860	0.0119344	0.0119327	1.7×10^{-6}
483.730	0.0119134	0.0119143	-9×10^{-7}
532.605	0.0118548	0.0118551	-3×10^{-7}
632.836	0.0117665	0.0117693	-2.8×10^{-6}
780.072	0.0116854	0.0116862	-8×10^{-7}
852.507	0.0116696	0.0116543	1.53×10^{-5}
975.079	0.0115978	0.0116065	-8.7×10^{-6}
1052.480	0.0115754	0.0115784	-3×10^{-6}
1064.100	0.0115677	0.0115743	-6.6×10^{-6}
1309.114	0.0114892	0.0114874	1.8×10^{-6}
1549.250	0.0114187	0.0113973	2.14×10^{-5}
1636.008	0.0113456	0.0113625	-1.7×10^{-5}

Table A.8: MgF_2 comparison between Sellmeier fit (Eq. 5.1, Table 5.12) and measured birefringence data. These data show a fit $<3.0 \times 10^{-6}$ prior to 850 nm, and a fit on the order of 2.0×10^{-5} at the last two data points, of 1549 nm and 1636 nm.

λ (nm, measured)	β (measured)
402.860	-0.0084792
444.814	-0.0083528
470.994	-0.0082899
483.864	-0.0082631
532.557	-0.0081813
588.058	-0.0081113
632.828	-0.0080684
780.079	-0.0079761
852.560	-0.0079477

Table A.9: Laser wavelengths and birefringence measurements for sapphire measured using polarimeter method.

λ (nm)	β (measured)	β (Sellmeier)	Δ
402.860	-0.0084792	-0.0084794	2×10^{-7}
444.814	-0.0083528	-0.008352	-8×10^{-7}
470.994	-0.0082899	-0.0082903	4×10^{-7}
483.864	-0.0082631	-0.0082637	6×10^{-7}
532.557	-0.0081813	-0.0081809	-4×10^{-7}
588.058	-0.0081113	-0.0081113	0
632.828	-0.0080684	-0.0080684	0
780.079	-0.0079761	-0.0079762	1×10^{-7}
852.560	-0.0079477	-0.0079477	0

Table A.10: Comparison of measured birefringence values and Sellmeier fit (Eq. 5.3, Table 5.14) for sapphire data taken on polarimeter. Fit is $<1.0 \times 10^{-6}$ for all wavelengths measured.

Quartz	MgF ₂	Sapphire
402.873 nm	402.732 nm	402.860 nm
450.966 nm	470.860 nm	444.814 nm
472.040 nm	483.730 nm	470.994 nm
483.437 nm	532.605 nm	483.864 nm
531.366 nm	632.836 nm	532.557 nm
588.054 nm	780.072 nm	588.058 nm
632.826 nm	852.507 nm	632.828 nm
781.873 nm	975.079 nm	780.079 nm
846.164 nm	1052.480 nm	852.560 nm
975.154 nm	1064.100 nm	-
1052.470 nm	1309.114 nm	-
1062.665 nm	1549.250 nm	-
1309.071 nm	1636.008 nm	-
1553.454 nm	-	-
1629.055 nm	-	-

Table A.11: Wavelengths tested on AxoScan and PAX polarimeters

Quartz	MgF ₂	Sapphire
-0.15	-0.34	-0.36

Table A.12: Change in effective thickness in microns of plates used in spectrophotometer due to non-collimated beam, at both 320 and 860 nm.

	Quartz	MgF ₂	Sapphire
320 nm	0.58	1.37	1.38
860 nm	0.61	1.40	1.45

Table A.13: Change in effective thickness in microns of plates used in spectrophotometer due to decrease in birefringence.

Material	Quartz	MgF ₂	Sapphire
Trendline R ² value	0.998	0.991	1.000

Table A.14: R² value of retardance versus temperature trendlines for materials. Lower value of R² for MgF₂ may be due to lower thickness of part used compared to other materials (see Table 4.3).

REFERENCES

- [1] Dale A. Holmes. Exact theory of retardation plates. *Journal of the Optical Society of America*, 1964.
- [2] Perkin Elmer. *Lambda 650/850/950 Hardware Guide*, 2004.
- [3] Shimadzu. Characteristics of single and double monochromator uv-vis spectrophotometers, 2024. https://www.ssi.shimadzu.com/service-support/technical-support/analysis-basics/fundamentals-uv/single_double.html, Last accessed 04-24-2024.
- [4] Gorachand Ghosh. Dispersion-equation coefficients for the refractive index and birefringence of calcite and quartz crystals. *Optics Communications*, 1999.
- [5] Marilyn J. Dodge. Refractive properties of magnesium fluoride. *Applied Optics*, 1984.
- [6] Irving H. Malitson and Marilyn J. Dodge. Refractive index and birefringence of synthetic sapphire. *Journal of the Optical Society of America*, 1972.
- [7] Michael Kraemer, Neil Rebolledo, and Tom Baur. Waveplate retardance metrology: The basics and beyond. Technical report, Meadowlark Optics, 2020.
- [8] Schott. Tie-29 refractive index and dispersion. Technical report, Schott, 2016.
- [9] Roger Chang. Application of polarimetry and interferometry to liquid crystal-film research. *Materials Research Bulletin*, 7, 1972.
- [10] Axometrics. Axoscan, 2024. <https://www.axometrics.com/products/polarimeters-ellipsometers/axoscan>, Last accessed 04-24-2024.
- [11] T Toyoda and M Yabe. The temperature dependence of the refractive indices of fused silica and crystal quartz. *Journal of Physics D: Applied Physics*, 1983.
- [12] Shelley M. Etzel, A. H. Rose, and C. M. Wang. Dispersion of the temperature dependence of the retardance in SiO_2 and MgF_2 . *Applied Optics*, 2000.
- [13] Michael E. Thomas, Stefan K. Andersson, Raymond M. Sova, and Richard I. Joseph. Frequency and temperature dependence of the refractive index of sapphire. *Infrared Physics and Technology*, 1998.
- [14] William L. Wolfe. More on the accurate measurement of refractive indices. *Applied Optics*, 1994.

- [15] Russell A. Chipman, Wai-Sze Tiffany Lam, and Garam Young. *Polarized Light and Optical Systems*. Taylor and Francis, 2019.
- [16] Mindat. Quartz, 2024. <https://www.mindat.org/min-3337.html>, Last accessed 04-24-2024.
- [17] Shinkosha. <https://www.shinkosha.com/english/techinfo/feature/>, Last accessed 04-24-2024.
- [18] T. M. Cotter, M. E. Thomas, and W. J. Tropf. Magnesium fluoride (mgf₂). In *Handbook of Optical Constants of Solids*. Academic Press, 1997.
- [19] N. Hagen, Kentaro Yoshida, Yuejin Shan, and Yukitoshi Otani. Apophyllite waveplates. *Applied Optics*, 2022.
- [20] Crystran. Crystal quartz sio₂, 2024. <https://www.crystran.co.uk/optical-materials/crystal-quartz-sio2>, Last accessed on 2024-02-26.
- [21] H. R. Gault. The frequency of twin types in quartz crystals. *American Mineralogist*, 1949.
- [22] S. Chandrasekhar. Theoretical interpretation of the optical activity of quartz. *Proceedings of the Indian Academy of Sciences*, 1953.
- [23] Rayotek. Transparent materials comparison, 2021. <https://rayotek.com/tech-specs/material-comparisons.htm>, Last accessed on 2024-01-24.
- [24] T. G. Golovina. Determination of the optical parameters of uniaxial optically active crystals taking into account the imperfection of spectrophotometric complex elements. *Crystallography Reports*, 2018.
- [25] D. Yang, M. E. Thomas, and S. G. Kaplan. Measurement of the infrared refractive index of sapphire as function of temperature. In *Proceedings of SPIE*, 2001.
- [26] Thorlabs. Precision measuring tools, 2024. https://www.thorlabs.com/newgrouppage9.cfm?objectgroup_id=1423, Last accessed on 2024-03-10.
- [27] Bristol Instruments. 157 series optical thickness gauge, 2024. <https://www.bristol-inst.com/bristol-instruments-products/thickness-gauges/157-series-optical-thickness-gauge/>, Last accessed on 2024-03-10.
- [28] A. Duncanson and R. W. H. Stevenson. Some properties of magnesium fluoride crystallized from the melt. *Proceedings of the Physical Society*, 1958.

- [29] A. C. DeFranzo and B. G. Pazol. Index of refraction measurement on sapphire at low temperatures and visible wavelengths. *Applied Optics*, 1993.
- [30] Michael Gartman and Meredith K. Kupinski. Birefringence measurements of crystal quartz, magnesium fluoride, and synthetic sapphire. *Proceedings of SPIE*, 2024.
- [31] D. C. Harris. A peek into the history of sapphire crystal growth. *Proceedings of SPIE*, 5078, 2003.
- [32] John E. Greinvenkamp. *Field Guide to Geometrical Optics*. SPIE, 2004.
- [33] PerkinElmer. Private communication, 2024. E-mail.